Semi-quantitative understanding of source contribution to nitrous acid (HONO) based on 1-year continuous observation at the SORPES station in eastern China

Yuliang Liu[1,2], Wei Nie[1,2*], Zheng Xu[1,2], Tianyi Wang[1,2], Ruoxian Wang[1,2], Yuanyuan Li[1,2], Lei Wang[1,2], Xuguang Chi[1,2], and Aijun Ding[1,2]

[1]Joint International Research Laboratory of Atmospheric and Earth System Sciences, School of Atmospheric Sciences, Nanjing University, Nanjing, Jiangsu Province, China

[2] Collaborative Innovation Center of Climate Change, Jiangsu Province, China

Abstract

Nitrous acid (HONO), an important precursor of the hydroxyl radical (OH), has been long-standing recognized to be of significance to atmospheric chemistry, but its sources are still debate. In this study, we conducted continuous measurement of HONO from November 2017 to November 2018 at the SORPES station in Nanjing of eastern China. The yearly average mixing ratio of observed HONO was 0.69 ±0.58 ppb, showing a larger contribution to OH relative to ozone with a mean OH production rate of 1.16 ppb/h. To estimate the effect of combustion emissions of HONO, the emitted ratios of HONO and NO_x were derived from 55 fresh plumes ($NO/NO_x > 0.85$), with a mean value of 0.79%. During the nighttime, the chemistry of HONO was found to depend on RH, and heterogeneous reaction of NO_2 on aerosol surface was presumably responsible for HONO production. The average nighttime NO_2-to-HONO conversion frequency (C_{HONO}) was determined to be 0.0055 ± 0.0032 h^{-1} from 137 HONO formation cases. The missing source of HONO around noontime seemed to be photo-induced with an average $P_{unknown}$ of 1.04 ppb h^{-1}, based on a semi-quantitative HONO budget analysis. An over-determined system of equations was applied to obtain the monthly variations in nocturnal HONO sources. Except for burning-emitted HONO (approximately 23% of total measured HONO), the contribution of heterogeneous formation on ground surfaces was an approximately

constant proportion of 36% throughout the year. The soil emission revealed clear seasonal variation, and contributed up to 40% of observed HONO in July and August. A higher propensity for generating HONO on aerosol surface occurred in heavily polluted period (about 40% of HONO in January). Our results highlight ever-changing contributions of HONO sources, and encourage more long-term observations to evaluate the contributions from varied sources.

1. Introduction

Nitrous acid (HONO) is a vital constituent of nitrogen cycle in the atmosphere, first observed in the field by Perner and Platt (1979). The concentrations of HONO varied from dozens of ppt in remote regions (Villena et al., 2011b;Meusel et al., 2016) to several ppb in polluted urban regions (Yu et al., 2009;Tong et al., 2015). The photolysis of HONO (R1) has been long standing as a momentous source of the hydroxyl radicals (OH) especially during the early morning when other OH sources are minor (Platt et al., 1980;Alicke, 2002, 2003). Even during the daytime, recent studies have recognized the photolysis of HONO as a potentially stronger contributor to daytime OH radicals than that of O_3 (Kleffmann, 2005;Elshorbany et al., 2009;Li et al., 2018). Meanwhile, HONO has been found to affect adversely human heath (Jarvis et al., 2005;Sleiman et al., 2010).

Although the significance of HONO has been given much weight, the sources of ambient HONO are complicated and have been debated for decades. HONO can be emitted from combustion, including vehicle exhaust, industrial exhaust and biomass burning (Table 1).Tunnel experiments with tests for different engine types have determined an emission ratio of HONO/NO_x for traffic source, ranged in 0.3-0.8% (Kirchstetter et al., 1996;Kurtenbach et al., 2001). The release from soil nitrite through acidification reaction and partitioning is considered to be another primary source of atmospheric HONO (Su et al., 2011). Soil nitrite could come from biological nitrification and denitrification processes (Canfield et al., 2010;Oswald et al., 2013), or be enriched via reactive uptake of HONO from the atmosphere

(VandenBoer et al., 2014a;VandenBoer et al., 2014b). In addition to direct emissions, the vast majority of HONO is produced chemically. The recombination of NO and OH (R3) is the main homogeneous reaction for supplying HONO (Pagsberg et al., 1997;Atkinson, 2000), whose contribution may be significant under conditions of sufficient reactants at daytime. During the nighttime, with low OH concentrations, other larger sources, i.e. heterogeneous reactions of NO_2 on various surfaces, are required to explain elevated mixing levels of HONO. Laboratory studies indicate that NO_2 can be converted to HONO on humid surfaces (R4), being first order in NO_2 and depending on various parameters including the gas phase NO_2 concentration, the surface water content, and the surface area density (Kleffmann et al., 1998;Finlayson-Pitts et al., 2003). Besides, the heterogeneous reduction of NO_2 with surface organics (R5) is proposed to be another effective pathway to generate HONO (Ammann et al., 1998;Ammann et al., 2005;Aubin and Abbatt, 2007), observed in freshly emitted plumes with high concentrations of NO_x and BC (Xu et al., 2015). Notably this reaction rate is drastically reduced after the first few seconds due to consumption of the reactive surfaces (Kalberer et al., 1999;Kleffmann et al., 1999), but this reaction could be strongly enhanced by light on photo-activated surface (George et al., 2005;Stemmler et al., 2006;Stemmler et al., 2007). During the daytime, heterogeneous HONO formation from the photolysis of adsorbed nitric acid (HNO_3) and particulate nitrate (NO_3^-) at UV wavelengths has been found in experiments and observations (Zhou et al., 2003;Zhou et al., 2011;Ye et al., 2016;Ye et al., 2017). Heterogeneous processes are typically considered as the primary sources of HONO in many regions yet are the most poorly understood. For NO_2 conversion to HONO on surfaces (R4,R5), the uptake coefficients of NO_2 derived from different experiments vary from 10^{-9} to 10^{-2} (Ammann et al., 1998;Kirchner et al., 2000;Underwood et al., 2001;Aubin and Abbatt, 2007;Zhou et al., 2015). The key step to determine the uptake of NO_2 or the reaction rate is still ill-defined, and we are also not certain if and how the ambient natural surfaces can be reactivated by radiation. Furthermore, it has become a main concern to compare the contributions of ground and aerosol surfaces to HONO formation. It is so far, not well explained for the observed HONO,

especially during daytime. Large unknown sources of HONO were identified by many studies (Su et al., 2008b;Sörgel et al., 2011;Michoud et al., 2014;Lee et al., 2016).

Benefitting from more and more studies, particularly the observations under different environments (Lammel and Cape, 1996;Li et al., 2012), understanding of HONO chemistry in the atmosphere has been greatly improved during the last decade. However, most HONO observations were short-term campaigns with studies ranging from several weeks to several months. For example, Reisinger (2000) found a linear correlation between the HONO/NO_2 ratio and aerosol surface density in the polluted winter atmosphere; and Nie et al. (2015) showed the influence of biomass burning plumes on HONO chemistry, according to observed data during late April–June 2012; while Wong et al. (2011) believed that NO_2 to HONO conversion on the ground was the dominant source of HONO by analyzing vertical profiles from15 August to 20 September in 2006. Moreover, a theory that HONO from soil emission explained the strength and diurnal variations of the missing source has been presented by Su et al. (2011) based on data measured from 23 to 30 October 2004. In case the HONO sources possibly exhibit temporal variability, especially seasonal differences, it is challenging to draw a full picture on the basis of these short-term observations. More than a year of continuous observation is needed, yet rather limited.

The Yangtze River Delta (YRD) is one of the most developed regions in eastern China. Rapid urbanization and industrialization have induced severe air pollution over the last three decades, particularly high concentrations of reactive nitrogen (Richter et al., 2005;Rohde and Muller, 2015), including HONO (Wang et al., 2013;Nie et al., 2015). In this study, we conducted HONO observations continuously from November 2017 to November 2018, at the Station for Observation Regional Processes and the Earth System (SORPES), located in the western part of the YRD, a place that can be influenced by air masses from different source regions of anthropogenic emissions, biomass burning, dust and biogenic emissions (Ding et al., 2013;Ding et al., 2016). Our one-year observation showed well-defined diurnal patterns and obvious season

variations of HONO concentrations at relatively high levels. We discussed the potential mechanism of HONO production based upon semiquantitative analysis and correlation studies, and paying special attention to changes in major sources of HONO during different seasons.

2. Methodology

2.1. Study site and instrumentation

Continuous observation was conducted at the SORPES station at the Xianlin Campus of Nanjing University (118°57′E, 32°07′N), located in the northeast suburb of Nanjing, China, from November 2017 to November 2018 (Fig. S1). The easterly prevailing wind and synoptic condition makes it a representative background site of Nanjing and a regional downwind site of the city cluster in the YRD region. Detailed descriptions for the station can be found in previous studies (Ding et al., 2013;Ding et al., 2016).

HONO was measured with a commercial long path absorption photometer instrument (QUMA, Model LOPAP-03). The ambient air was sampled in two similar temperature controlled stripping coils in series using a mixture reagent of 100 g sulfanilamide and 1 L HCl (37% volume fraction) in 9 L pure water. In the first stripping coil, all of the HONO and a fraction of interfering substances were absorbed into solution, and the remaining interfering species (NO_2, HNO_3, HO_2NO_2, PAN, etc.) were absorbed in the second stripping coil. After adding a reagent of 0.8 g N-naphtylethylendiamine-dihydrochloride in 8 L pure water to, colored azo dyewas formed in the solutions from 2 stripping coils, which were then separately detected via long path absorption in special Teflon tubing. To minimize the measurement interferences, the real HONO signal was the difference between the signals in the two channels. Further details can be found in (Heland et al., 2001;Kleffmann et al., 2006). To correct for the small drifts in instrument's baseline, the compressed air was sampled every 12 h (flow rate: 1.0 L/min) to make zero measurement. A span check was made using 0.04 mg/m^3 nitrite (NO_2^-) solution each two weeks with a flow rate of

0.28 ml/min. The time resolution, detection limit, accuracy of the measurement was 5 min, 10 pptv, and 10%, respectively.

The NO and NO_2 levels were measured using a chemiluminescence instrument (TEI, model 42i) coupled with a highly selective photolytic converter (Droplet Measurement Technologies, model BLC), and the analyzer had a detection limit of 50 pptv for an integration time of 5 min, with precision of 4% and an uncertainty of 10% (Xu et al., 2013). Ozone and CO were measured continuously using Thermo-Fisher Scientific TEI 49i and TEI 48i, respectively. The fine particle mass concentration ($PM_{2.5}$) was continuously measured with a combined technique of light scattering photometry and beta radiation attenuation (Thermo Scientific SHARP Monitor Model 5030). Water soluble aerosol ions (NO_3^-, SO_4^{2-}, NH_4^+ etc.) and ammonia (NH_3) were measured by a Monitor for Aerosols and Gases in ambient Air (designed and manufactured by Applikon Analytical B.V., the Netherlands) with a $PM_{2.5}$ cyclone inlet, in a time resolution of 1 hr. The size distribution of submicron particles (6-820 nm) is measured with a DMPS (differential mobility particle sizer) constructed at the University of Helsinki in Finland. Meteorological measurements including relative humidity (RH), wind speed, wind direction, and air temperature were recorded by Automatic Weather Station (CAMPEEL co., AG1000). UVB total radiation was measured by UVB radiometer (UVS-B-T UV Radiometer, KIPP &ZONEN).

2.2. TUV model and OH estimate

The Tropospheric Ultraviolet and Visible (TUV) Radiation Model (http://www.acd.ucar.edu/TUV) was adopted to compute the photolysis frequencies, which is most probably accurate in clean and cloudless days. The pivotal parameters of this model were inputted as follows: the ozone density was measured by Total Ozone Mapping Spectrometer (http://toms.gsfc.nasa.gov/teacher/ozoneoverhead.html); the typical single scattering albedo (SSA) and Ångström exponent (Alpha) were 0.93 and 1.04 (Shen et al., 2018); The mean value of optical depth (AOD) at 550nm was 0.64, derived following an empirical relationship with $PM_{2.5}$ in Nanjing (Shao et al.,

2017). To reduce the error of model, we used observed UVB to correct simulated results (J_{mod}) by Eq. (1).

$$J = \frac{UVB_{obs}}{UVB_{mod}} J_{mod} \quad (1)$$

The daytime OH concentration was calculated by applying the empirical model (Eq. 2) proposed by Rohrer and Berresheim (2006), based on strong nearly linear correlations of measured OH concentrations with simultaneously observed $J(O^1D)$. The coefficient **a** reflects the average influence of reactants (e.g. NO_x, VOCs, ozone, H_2O) on OH at the selected place for research; the exponent **b** represents the combined effects of all photolytic processes on OH, for example, $J(O^1D)$, $J(NO_2)$, J(HONO), J(HCHO) and so on; and the parameter **c** counts the light-independent OH sources. The values of coefficients **a**, **b** and **c** in Eq. (2) are adopted from the OH studies in the Pearl River Delta (PRD) and Beijing, China (Rohrer et al., 2014;Tan et al., 2017;Tan et al., 2018). By summarizing the coefficients **a**, **b**, **c** in different OH observation campaigns (Table S1), especially the almost equal slope of the OH-$J(O^1D)$ relation for different locations and seasons in the polluted areas of China, we can make assumptions that the comprehensive impact of reactants (e.g. NO_x and VOCs) on OH cannot compete with that of UV light to OH, and the chemical environments of OH are similar. This suggest that it can be a reasonable way to derive OH by using Eq. (2) in our study, and the error of derived OH radicals has been assessed as not subverting the relative conclusions in this study (Fig. S1(a) and Fig. S1(d)). The calculated OH concentrations around noon ($J(O^1D)>1\times10^{-5}$ s^{-1}) were in the range of $0.46\text{-}2.0\times10^7$ cm^{-3}, comparable to observations in Chinese urban or suburban atmospheres (Lu et al., 2012;Lu et al., 2013).

$$[OH] = a \times (J(O^1D)/10^{-5}s^{-1})^b + c$$
$$a=4.2\times10^6 cm^{-3},\ b=1$$
$$c = 1.0\times10^6 cm^{-3} \text{ in summer} \quad (2)$$
$$c = 0.6\times10^6 cm^{-3} \text{ in spring, autumn}$$
$$c = 0.2\times10^6 cm^{-3} \text{ in winter}$$

3. Results

3.1. Observation overview

We carried out continuous measurements for HONO at the SORPES station in the northeast suburb of Nanjing from November 2017 to November 2018 with a mean measured ambient HONO mixing level of 0.69 ±0.58 ppb (Fig. S2), within the range of those in or in the vicinity of mega cities (Table 2). Fig.1 shows the seasonal pattern of HONO and related parameters. The highest concentration of HONO was found in winter (1.04 ± 0.75 ppb), followed by spring (0.68 ± 0.48 ppb), autumn (0.66 ±0.53 ppb) and summer (0.45 ± 0.37 ppb). Such seasonal variations in Nanjing are aligned with that in Beijing (Hendrick et al., 2014), and are somewhat similar to those in Jinan (Li et al., 2018), where the highest levels occurred in winter and the lowest levels occurred in autumn, but these variations are different from those in Hongkong (Xu et al., 2015) where the highest and lowest values of HONO appeared in autumn and spring, respectively. The important point is that the seasonality of HONO coincides with that of NO_x (or NO_2), which is believed to be the main precursor of HONO in current studies.

The HONO to NO_x ratio or the HONO to NO_2 ratio has been used extensively in previous researches to characterize the HONO levels and to indicate the extent of heterogeneous conversion of NO_2 to HONO, since it is less influenced by convection or transport processes than the individual concentration (Lammel and Cape, 1996;Stutz et al., 2002). When a large proportion of HONO comes from direct emissions, the value of $HONO/NO_2$ usually becomes larger, falsely implying the strong formation of HONO from NO_2. However, the freshly emitted air masses

generally have the lowest HONO/NO_x ratio, meaning that HONO/NO_x behaves better than HONO/NO_2 in a way. As shown in Fig. 1(b), the low value of HONO/NO_x in winter is attributed to heavy emissions because we see high mixing ratios of NO during this cold season (Fig. 1c), the reasons for two peaks of HONO/NO_x in spring and summer will be discussed in sections 3.3, 3.4 and 4.

All daily changes of HONO concentration in different seasons closely resemble a cycle where HONO peaks in the early morning, and then decreases to the minimum in the late afternoon, following the diurnal trend of NO_x (Fig. 2). The daily variations of HONO in Nanjing are like those seen in other urban areas (Villena et al., 2011a;Wang et al., 2013;Michoud et al., 2014;Lee et al., 2016), but differ from observations on the roadside (Rappenglück et al., 2013;Xu et al., 2015). At night, the mixing ratio of HONO increases rapidly in the first few hours and then stabilizes (in spring and summer) or gradually climbs to its peak in the morning rush hour (in winter and autumn). The accumulation during nighttime hours suggests a significant production of HONO exceeding the dry deposition of HONO. As the sun rises, the HONO sink will be strengthened by photolysis and the vertical mixing processes, resulting that the peak times of the diurnal patterns of HONO concentration varies in different seasons. During the daytime, the rate of HONO abatement is rapid before noon and then becomes progressively until HONO concentration falling to the minimum. Given that the photolytic lifetime of HONO is about 10-20min at the midday (Stutz et al., 2000), the considerable HONO concentration during daytime indicates the existence of strong production of HONO.

From the daily variations of the HONO to NO_x ratio, we can further understand the behavior of HONO in the atmosphere. the HONO/NO_x ratio is regularly enhanced quickly before midnight then reaches a maximum during the latter half of the night. According to Stutz et al. (2002), the highest HONO/NO_x (or HONO/NO_2) is defined by the balance between production and loss of HONO at each night, the conditions affecting the highest achievable ratio at nighttime will be discussed in section 3.3.

What's interesting here is the peak of the HONO/NO_x ratio in the midday sun in spring, summer and autumn, and even in winter, the ratio doesn't decline but remains stationary before and at noon. If the HONO sources during the daytime are consistent with those at night, the minimum HONO/NO_x ratio should occur at noon due to the intense photochemical loss of HONO. Therefore, there must be additional sources of HONO during daytime (e.g. R3). The increase of HONO/NO_x with solar radiation (e.g., UVB) is found in both diurnal and seasonal variations, indicating that these daytime sources have a relationship with the intensity of solar radiation. We will further discuss the potential daytime sources of HONO in section 3.4.

The elevated mixing ratio of HONO presents an efficient source of OH radicals during daytime in Nanjing. We calculate the OH production rate from HONO, i.e. P_{OH}(HONO), using Eq. (3). As discussed in Su et al. (2008b) and Li et al. (2014), HONO produced by the reaction of NO with OH (R3) is actually a temporary reservoir of OH radicals. The photolysis of HONO from this pathway only regenerates OH radicals, cannot contribute to the concentrations of OH radicals. So it is inappropriate to estimate the primary OH production from HONO based on P_{OH}(HONO) derived from Eq. (3). For comparison, the OH production rate from ozone photolysis, $P_{OH}(O_3)$, is derived from Eq. (4). Only part of the $O(^1D)$ atoms, formed by the photolysis of O_3 at wavelengths below 320 nm (R7), can produce OH radicals by reacting with water (R8) in the atmosphere, so we use the absolute water concentration, which can be derived from relative humidity and temperature, to calculate the branching ratio of $O(^1D)$(ϕ_{OH}) between R8 and R9. The reaction rate of $O(^1D)$ with O_2 is 4.0×10^{-11} cm^3 $molecules^{-1}$ s^{-1} and the reaction rate of $O(^1D)$ with N_2 is 3.1×10^{-11} cm^3 $molecules^{-1}$ s^{-1} (Seinfeld and Pandis, 2016). In addition to the two mechanisms mentioned above, there are other pathways to generate primary OH radicals: the photolysis of aldehydes, mainly HCHO, can form HO_2 radicals, and then converting to OH radicals by reacting with NO; the reactions of ozone with alkenes produce OH radicals directly (Finlayson-Pitts and Pitts, 2000;Seinfeld and Pandis,

2016).

$$P_{OH}(HONO) = J(HONO)[HONO] \quad (3)$$

$$P_{OH}(O_3) = 2J(O^1D)[O_3]\phi_{OH} \quad (4)$$
$$\phi_{OH} = k_8[H_2O]/(k_8[H_2O] + k_9[M])$$

$$O_3 + h\upsilon \rightarrow O(^1D) + O_2(\lambda < 320nm) \quad (R7)$$

$$O(^1D) + H_2O \rightarrow 2OH \quad (R8)$$

$$O(^1D) + M \rightarrow O(^3P) + M \ \ (M \text{ is } N_2 \text{ or } O_2) \quad (R9)$$

Fig. 3 shows that the diurnal peak of OH production rate from HONO is usually found in the late morning, caused by the combined effects of HONO concentration and its photolysis frequency, and the seasonal peak of P_{OH}(HONO) occurs in spring for the same reason. $P_{OH}(O_3)$, coinciding with the trend of $J(O^1D)$, is highest around noon at daily time scale and is highest in summer at seasonal time scale, respectively. Significantly, the photolysis of HONO produce more OH than that of ozone throughout the daytime in winter, spring, and autumn. In summer, the contribution of HONO to OH is greater in the early morning, and although the photolysis of ozone contributes more OH at noon, the role of HONO is considerable. Overall, the average P_{OH}(HONO) during 8:00-16:00 LT is 1.16 ppb/h, and the mean value of $P_{OH}(O_3)$ is 0.41 ppb/h. The impressive role of HONO in the atmospheric oxidizing capacity should benefit photochemical ozone production (Ding et al., 2013;Xu et al., 2017;Xu et al., 2018), new particle formation (Qi et al., 2015) and secondary aerosol formation (Xie et al., 2015;Sun et al., 2018) in Nanjing, the western YRD region.

3.2. Direct emissions of HONO from Combustion

As mentioned above, the good correlation of HONO with NO_x (Fig. 4a) and the similar patterns of HONO and NO_x, particularly sharply increasing together in the fresh plumes, in which the NO/NO_x ratios are usually very high (Fig. S2), indicate the presence of direct combustion emission of HONO, which need to be deducted when

analyzing the secondary formation of HONO. The SORPES station is influenced by air masses from both industries and vehicles (Ding et al., 2016), so the traffic emission factor investigated in other experiments cannot be used straightly. We derive the emitted HONO/NO_x ratio according the method of Xu et al. (2015), and the following criteria are adopted to select fresh plumes: (a) [NO_x]>40 ppbv; (b) $\triangle NO/\triangle NO_x > 0.85$; (c) good correlation between HONO and NO_x (r>0.9); (d) short duration of plumes (<=2 h); and (e) [UVB]<=0.01 W/m^2. Then, the slopes of HONO to NO_x in selected plumes were considered as the emission ratios in our study.

Within the one-year dataset, we select 55 freshly emitted plumes satisfying the criteria above (Table S2), of which 20 air masses were found in the morning and evening rush hours; the derived $\triangle HONO/\triangle NO_x$ ratios vary from 0.26% to 1.91% with a mean value of 0.79%±0.36%. Many factors, such as the amount of excess oxygen; the types of fuel used (gasoline, diesel, coal); if engines are catalyst-equipped, and if engines are well-maintained, could result in variances in these ratios. Additionally, the rapid heterogeneous reduction of NO_2 on synchronously emitted BC can also raise the value of $\triangle HONO/\triangle NO_x$ (Xu et al., 2015). For our study, an average emission factor of 0.79% is deployed to evaluate the emission contribution of HONO (Eq. 5), which is abbreviated as $HONO_{emis}$.

$$HONO_{emis} = NO_x \times 0.0079 \quad (5)$$

$$HONO_{corr} = HONO - HONO_{emis} \quad (6)$$

Combustion emissions contribute an average of 23% of total measured HONO concentrations at night (Fig. 4b), with a maximum $HONO_{emis}$/HONO value of 32% in winter and a minimum $HONO_{emis}$/HONO value of 18% in summer. We then get the corrected observed HONO ($HONO_{corr}$) by Eq.(6) for further analysis. The slope of the fitted line for HONO and NO_x is 1.62%, higher than emission ratio 0.79% (Fig. 4a), and almost 80% of HONO is from $HONO_{corr}$ that is not affected by emissions (Fig. 4b). These imply significant secondary formation of HONO in the atmosphere.

3.3. Heterogeneous conversion of NO_2 to HONO during at nighttime

3.3.1. The NO_2-to-HONO conversion rate (C_{HONO})

In addition to emissions, heterogeneous reaction of NO_2 on surfaces (R4, R5) is believed to be the major formation pathways of nocturnal HONO. Thus, the NO_2-to-HONO conversion rate is calculated from Eq. (5) (Alicke et al., 2002;Alicke, 2003;Wentzell et al., 2010), where NO_2 is adopted to scale HONO to reduce the dilution influence according to Su et al. (2008a). Similar to HONO/NO_x (Fig. 2), the nighttime $HONO_{corr}/NO_2$ ratio rises from the lowest value and then reaches a quasi-stable state, meaning that C_{HONO} can actually be used to assess how quickly $HONO_{corr}/NO_2$ can increase to its equilibrium.

$$C_{HONO} = \frac{\frac{[HONO_{corr}]_{(t_2)}}{[NO_2]_{(t_2)}} - \frac{[HONO_{corr}]_{(t_1)}}{[NO_2]_{(t_1)}}}{t_2 - t_1} \quad (7)$$

Following the method of Xu et al. (2015) and Li et al. (2018), 137 cases in which $HONO_{corr}/NO_2$ increased almost linearly from 18:00 to 24:00 each night are selected, and the slope fitted by the least linear regression for $HONO_{corr}/NO_2$ against time is just the conversion frequency of NO_2 to HONO. The derived C_{HONO} vary from 0.0043±0.0017 h^{-1} in winter to 0.0066±0.0040 h^{-1} in summer, with an average value of 0.0055±0.0032 h^{-1}, which is in the range (0.004-0.014 h^{-1}) shown by other studies in urban and suburban sites (Fig. 5). Noting that C_{HONO} assumes all the increase of $HONO_{corr}/NO_2$ is caused by the conversion of NO_2, excluding other possible sources of HONO (e.g. soil nitrite); and the computed C_{HONO} is the net NO_2-to-HONO conversion rate since the measured $HONO_{corr}$ has already taken the sinks of HONO (mainly deposition) into account. Considering the uncertainties of C_{HONO}, utilizing C_{HONO} directly to analyze the mechanism of HONO formation thoroughly may not be appropriate, but it could be attemptable to facilitate the parameterizations for HONO production in air quality models by C_{HONO} when the chemical mechanisms are not

clear yet.

3.3.2. RH dependence of HONO chemistry

It appears that NO_2 hydrolysis on humid surfaces (R4), having a first order dependence on NO_2 (Jenkin et al., 1988;Ackermann, 2000;Finlayson-Pitts et al., 2003), is influenced by the surface absorbed water (Kleffmann et al., 1998;Finlayson-Pitts et al., 2003), although the exact mechanisms are still unknown. In the studies of Stutz et al. (2002) and Stutz et al. (2004), the pseudo steady state of $HONO/NO_2$, where this ratio is at a maximum at nighttime, is presumed to be a balance between the production of HONO from NO_2 and the loss of HONO on surfaces, and the highest $HONO/NO_2$ value is determined by the ratio of the reactive uptake coefficients for each process. Scatter plot of $HONO_{corr}/NO_2$ against relative humidity in our study are illustrated in Fig. 6. To eliminate as much influence of other factors as possible, the average of the 6 highest $HONO_{corr}/NO_2$ values in each 5% RH interval is calculated, according to Stutz et al. (2004). The phenomenon that $HONO_{corr}/NO_2$ first increases and then decreases with an increasing RH in Fig. 6(a) was also observed by other studies (Hao et al., 2006;Yu et al., 2009;Li et al., 2012;Wang et al., 2013). The dependencies of $HONO_{corr}/NO_2$ on RH and the possible reasons or mechanisms are discussed as follows. Even at the lowest measured RH of 18%, the absolute moisture content in the atmosphere is still greater than 10^3 ppm in our study, which is quite abundant to react with NO_2, but the $HONO_{corr}/NO_2$ ratio is quite small and remains unchanged when RH is below 45%, indicating that the NO_2 to HONO conversion efficiency should be determined by water covering the surfaces, rather than by the amount of water in the air.

It has been reported that surfaced absorbed water depends on RH values, and the dependences vary for different material surfaces of the ground, but generally follow the shape of a BET isotherm (Lammel, 1999;Saliba et al., 2001;Sumner et al., 2004). The number of mono-layers of water increases slowly from zero to 2-4, accompanied by RH from zero to a turning point, and the water coverage grows dramatically (up to

10-100 mono-layers) once RH exceeds the turning point (Finlayson-Pitts et al., 2003). Fig. 6(a) shows the case where the surface for NO_2 converting to HONO is dominated by the ground, the $HONO_{corr}/NO_2$ increases along with RH when RH is less than 75%, which can be explained by the reaction of NO_2 to generate HONO on wet surfaces. However, a negative correlation between $HONO_{corr}/NO_2$ and RH is found when RH is over 75%, presumably because that the rapidly growing aqueous layers of the ground surface lead to efficient uptake of HONO and make the surface less accessible or less reactive for NO_2. Hence, the RH turning point for absorbed water on ground surfaces is perhaps around 75% for our observation, within the range of results from experiments on various surfaces (70-80% RH) (Lammel, 1999;Saliba et al., 2001;Sumner et al., 2004). Once RH exceeds 95%, the reaction surface is asymptotically approaching the state of water droplet, where the quite limited formation of HONO and the extremely impactful loss of HONO will result in a dramatic decline of the $HONO_{corr}/NO_2$ ratio (Fig. 6(a) and Fig. 6(b)).

Notably, the constant $HONO_{corr}/NO_2$ value at RH between 75-95% under the condition of high $PM_{2.5}$ mass loading (Fig. 6(b)), compared to the downward trend of $HONO_{corr}/NO_2$ within the same humidity range in low $PM_{2.5}$ mass concentration (Fig. 6(a)), implies a contribution of aerosol surfaces to the NO_2-HONO conversion. Since both $HONO_{corr}/NO_2$ in Fig. 6(a) and Fig. 6(b) are affected by the ground surfaces, we can use the difference of $HONO_{corr}/NO_2$ between the two figures to represent the influence of aerosol. As the area of shadow showed in Fig. 6(b), the aerosol-affected $HONO_{corr}/NO_2$ is positively related to RH before RH reaches 95%. With the increase of RH, the hygroscopic growth of aerosol particles should provide larger surface area. When RH is higher than 75%, which has exceeded the mutual deliquescence relative humidity of inorganic salts (Fountoukis and Nenes, 2007), aerosols will transfer to aqueous phase gradually, and then promoting multiphase or heterogeneous chemistry processes (Herrmann et al., 2015). For example, the oxidation of SO_2 by NO_2 on aqueous aerosol surface may produce NO_2^-/HONO efficiently under polluted condition (Xie et al., 2015;Wang et al., 2016). In addition, the enhancement NO_2

uptake on micro-droplets by anions has been reported in experiments (Yabushita et al., 2009)

3.3.3. Impact of aerosols on HONO formation

To further understand the heterogeneous formation of HONO on aerosol, we carry out a correlation analysis when $HONO_{corr}/NO_2$ reaches the pseudo steady state at each night (3:00-6:00 LT). The convergence or diffusion processes of gases and particles caused by the decrease or increase of the boundary layer height can also lead to a consistent trend of $HONO_{corr}$ and $PM_{2.5}$ (Fig. 7a), while the ratio of $HONO_{corr}$ and NO_2 can not only reduce this physical effect but also represent the conversion degree of NO_2 to HONO, so a moderate positive correlation between $HONO_{corr}/NO_2$ and $PM_{2.5}$ (r=0.35, p=0.01) throughout the observation period could be more convincible (Fig. 7b). As shown by larger triangles with gray borders in Fig. 7(b), $HONO_{corr}/NO_2$ is better correlated with $PM_{2.5}$ in the months when the mass concentrations of $PM_{2.5}$ are higher during this 1-year measurement, generally occurring from November to May (Fig. 1d).This finding can be explained with a law that greater contributions of NO_2 heterogeneously reacting on aerosol surface to HONO cause better correlations between $HONO_{corr}/NO_2$ and $PM_{2.5}$. Interestingly, this relationship can also be divided approximately into two groups by NH_3/CO; the correlation is good when the value of NH_3/CO is lower than 2‰, but when NH_3/CO is higher than 2‰, a poor correlation is found. We will discuss this phenomenon further in section 4. The evidence of HONO formation on aerosol were also found in other observations (Reisinger, 2000;Wang, 2003;Li et al., 2012;Nie et al., 2015;Hou et al., 2016;Cui et al., 2018).

As is known, producing HONO is not the dominant sink of NO_2 at night, but it seems that more NO_2 can be converted to HONO under conditions of heavy pollution (Fig. 7b). We discuss whether heterogeneous reactions of NO_2 on aerosols are able to provide comparable HONO with our measurement by Eq. (8), only considering HONO formation on particle surfaces and assuming that HONO principally settles on

478 the ground surface, neglecting HONO loss on aerosol. c_{NO_2} is the mean molecular
479 velocity of NO_2 (370m/s); $[\frac{S}{V}]_{aer}$ is the surface area to volume ratio (m^{-1}) of aerosol;
480 ν_{HONO} is the deposition velocity of HONO, which is considered to be close to the
481 deposition velocity of NO_2 at night (Stutz et al., 2002;Su et al., 2008a); and a
482 approximate value of 0.1cm/s is used based on the measurements from Coe and
483 Gallagher (1992) and Stutz et al. (2002); H is the boundary layer mixing depth, and a
484 value of 100m is assumed for nighttime (Su et al., 2008a).
485
486 $$C_{HONO} = \frac{1}{4}\gamma_{NO_2\rightarrow HONO} c_{NO_2} [\frac{S}{V}]_{aer} - \frac{\nu_{HONO}}{H}\frac{[HONO]}{[NO_2]} \quad (8)$$
487
488 Considering at nighttime period with severe haze, the aerosol surface density
489 calculated from the particle number size distributions between 6 nm and 800 nm is
490 about 1.2×10^{-3} m^{-1}, matched by 200 $\mu g/m^3$ of $PM_{2.5}$ from our observations, and the
491 averaged mixing ratios of HONO and NO_2 are 1.15 ppb and 28.4 ppb, respectively
492 (Table 2). For 30%-100% of the measured mean C_{HONO} (0.0043 h^{-1}) in winter, the
493 uptake coefficient of NO_2-to-HONO ($\gamma_{NO_2\rightarrow HONO}$) calculated from Eq. (8) is in the range
494 of 6.9×10^{-6} to 1.44×10^{-5}, consistent with the results from many laboratory studies
495 which demonstrate that the uptake coefficients of NO_2 (γ_{NO_2}) on multiple aerosol
496 surfaces or wet surfaces are mainly distributed around 10^{-5} with the HONO yield
497 varying from 0.1 to 0.9 (Grassian, 2002;Aubin and Abbatt, 2007;Khalizov et al.,
498 2010;Han et al., 2017). It is necessary to elaborate that: (1) the ambient particles were
499 dried with silica gel before measuring their number size distributions, and the mass
500 concentrations of $PM_{2.5}$ were also measured under a system where the temperature
501 was maintained at 30℃, usually above ambient temperature; (2) the aerosol surface
502 was calculated by assuming that all particles are spherically shaped, but the particles
503 could in fact have irregular bodies and porous structure; (3) the particle size of both

$PM_{2.5}$ and derived $[\frac{S}{V}]_{aer}$ is just a part of the total suspended particulate matter. As described, the aerosol surface in the atmosphere is actually underestimated in our study, thus the $\gamma_{NO_2 \rightarrow HONO}$ we derived could be the upper limit of the uptake coefficient for NO_2 conversion to HONO on aerosol. In addition to particles surfaces, other aerosol parameters such as surface water content, chemical composition, pH value, and phase state of surfaces may also influence the heterogeneous formation of HONO.

3.4. Missing daytime HONO source

After discussing the nocturnal formation mechanism of HONO, we now focus on the chemistry of daytime HONO whose concentrations are still about 0.25-0.6 ppb at noon with a lifetime of only 10-20 min (Fig. 2). We are not certain if the observed HONO can be provided by known mechanisms (gas phase reaction (R4) and emissions) to date, so a budget equation of daytime HONO (Eq. 9) is utilized to analyze its source and sinks (Su et al., 2008b;Sörgel et al., 2011). Here, dHONO/dt is the change rate of the observed HONO. The sources rates of HONO contain the homogeneous formation rate (P_{NO+OH}, R3); the combustion emission rate (P_{emis}); and the unknown HONO daytime source ($P_{unknown}$). The sink rates of HONO consist of the photolysis rate (L_{phot}, R1); the reaction rate of HONO with OH ($L_{HONO+OH}$, R2); and the dry deposition rate (L_{dep}). T_V and T_h represent the vertical (T_V) and horizontal (T_h) transport processes of HONO, which are thought to be negligible for intense radiation and relatively homogeneous atmospheres with generally calm winds (Dillon, 2002;Su et al., 2008b;Sörgel et al., 2011).

$$\frac{dHONO}{dt} = (P_{NO+OH} + P_{emis} + P_{unknown}) - (L_{phot} + L_{HONO+OH} + L_{dep}) + T_v + T_h \qquad (9)$$

Therefore, the undiscovered daytime source of HONO ($P_{unknown}$) can be derived by Eq. (10), which is a deformation of Eq. (9) without minor terms (T_v and T_h) and where

dHONO/dt is substituted by ΔHONO/Δt that is counted as difference between observed HONO at two time points. The reaction rate constants of reaction 2 ($k_{HONO+OH}$) and reaction 3 (k_{NO+OH}) are 6.0×10^{-12} cm^3 $molecules^{-1}$ s^{-1} and 9.8×10^{-12} cm^3 $molecules^{-1}$ s^{-1}, respectively (Atkinson et al., 2004). The emission ratio of HONO and NO_x ($HONO/NO_x$=0.79%) obtained in section 3.2, is used to estimate P_{emis}. For L_{dep}, the dry deposition velocity of diurnal HONO (ν_{HONO}) is measured as 2cm/s in the work of Harrison et al. (1996), and a practical mixing height of 200m is adopted, considering that most of the HONO cannot rise above this altitude due to rapid photolysis (Alicke et al., 2002). Although we did not observe OH radicals directly, the uncertainty of $P_{unknown}$ caused by the calculated OH radicals from Eq. (2) can be reduced substantially in the case of low concentration of NO and high value of $J(O^1D)$ (Fig. S1(d)).

$$P_{unknown} = J(HONO)[HONO] + k_{HONO+OH}[HONO][OH] + \frac{\nu_{HONO}}{H}[HONO] + \frac{\Delta HONO}{\Delta t} - k_{NO+OH}[NO][OH] - \frac{0.79\% \times \Delta NO_x}{\Delta t} \quad (10)$$

Fig. 8 shows the average daytime HONO budget from 8:00 LT to 16:00 LT during different seasons. The major loss route of HONO is photodecomposition (L_{phot}) with an average value of 1.50 ppb/h around noontime (10:00-14:00 LT) during this observation period, next to dry deposition (L_{dep}) whose mean value at the same time is 0.21 ppb/h, and by $L_{HONO+OH}$ which is less than 5% of that of L_{phot}. For the sources of HONO around noon, the average homogeneous reaction rate between NO and OH (P_{NO+OH}) is 0.63 ppb/h and P_{emis} just gives a tiny part of HONO at a rate of 0.02 ppb/h, meaning that most of HONO comes from an unknown source whose average rate ($P_{unknown}$) is 1.04 ppb/h, contributing about 61% of the production of HONO. Comparing summer data, the mean unknown daytime source strength of HONO in Nanjing is almost at the upper-middle level of those reported in the existing literature: 0.22 ppb/h at a rural site of New York state, USA (Zhou et al., 2002); 0.5 ppb/h in a forest near Jülich, Germany (Kleffmann, 2005); 0.77 ppb/h in a polluted rural area of

the Pearl River Delta, China (Li et al., 2012); 0.98 ppb/h at an urban site in Xi'an, China (Huang et al., 2017); 1.7 ppb/h in an urban area of Santiago, Chile (Elshorbany et al., 2009); 2.95 ppb/h in the urban atmosphere of Jinan, China (Li et al., 2018). In our study, the OH production rate from the missing HONO accounts for about 53% of total P_{OH}(HONO) (Fig. S2), suggesting that the unconventional source of HONO is of significance to atmospheric oxidation.

Hence, we perform a correlation analysis to explore the potential unknown daytime mechanisms of HONO (Table 3). $P_{unknown}$ is better correlated with NO_2*UVB than with NO_2 or UVB alone in winter, spring and autumn (p=0.05), perhaps associated with the photo-enhanced conversion from NO_2 to HONO (George et al., 2005;Stemmler et al., 2006;Stemmler et al., 2007). The average value of $P_{unknown}$ normalized by NO_2 is 0.1 h^{-1}, over 18 times greater than the nighttime conversion rate (0.0055 h^{-1}), also implying that $P_{unknown}$ cannot be explained by the nocturnal mechanism of NO_2-to-HONO. Assuming that the height of a well-mixed boundary layer around noon remains constant for each day, UVB*NO_2 and UVB*NO_2*$PM_{2.5}$ could be proxies for photo-induced heterogeneous reactions of NO_2 on ground and aerosol surfaces, respectively. We do not have any solid evidence to identify which surfaces (ground or aerosol) are more important to the photo-heterogeneous reaction of NO_2 based on the present analysis. For the same reason, the photolysis of particulate nitrates (NO_3^-) as a source of HONO (Ye et al., 2016;Ye et al., 2017) cannot be determined whether it is momentous in our study. The comparisons of correlation coefficients showed above follow the method provided by Meng et al. (1992).

Our study suggest that the missing source of HONO should be considered in the air quality forecasting or regional models to characterize atmospheric oxidizing capacity better, especially in warm seasons (spring and summer). Based on the measurement (Fig. S3), the light-induced heterogeneous conversion of NO_2 to HONO on aerosol surfaces and ground surface can been included in simulation works probably, as what

did in Lee et al. (2016).

4. Semi-quantitative estimation of the contribution from different sources

From this and previous studies, we can conclude that not only the concentration of ambient HONO but also the sources of HONO have temporal and spatial patterns, which is supposed to be considered in model studies. Nocturnal HONO is selected to discuss the monthly variations of HONO sources in detail without the uncertainties of daytime HONO formation, the influences of HONO photolysis, and the mixing effect of boundary layer. The heterogeneous reaction of NO_2 on aerosol produces a considerable portion of HONO in relatively polluted months (Dec.-May), but contributes very little less than nothing in clean months (Jun.-Oct.), as seen in section 3.3.3. Coincidentally, direct emissions from burning processes of HONO decrease from their peak values from winter to summer (section 3.2). However, the monthly averaged ratios of HONO and NO_x are highest in summer, which conflicts with the two sources mentioned above.

As is known, higher NO_2-to-HONO conversion level or other NO_x-independent sources can cause an increase in the HONO/NO_x ratio. For the case of a mostly constant surface with low reactivity due to the prolong exposure to oxidizing gases and radiation, the yield of nighttime HONO from NO_2 reacting on ground surfaces could be imprecisely assumed to be unchanged. Thus, soil nitrite formed through microbial activities, especially nitrification by ammonia-oxidizing bacteria ($NH_4^+ \rightarrow NO_2^-$) (Su et al., 2011;Oswald et al., 2013), is adopted to be an source for atmospheric HONO in this study, considering the nearby presence of some grassland and natural vegetation mosaics. Although we do not directly measure HONO emissions from soil, the observed ammonia can represent its monthly average intensity indirectly, based on the following hypothesis: the dominant source of NH_3 is from soil, especially from fertilizers ($NH_4^+ \rightarrow NH_3$) for a good correlation between ammonia and temperature in the site ($r=0.63$, $p=0.01$), omitting the contributions of livestock to NH_3 since there is only a small poultry facility within 10 km of this site

(Meng et al., 2011;Huang et al., 2012;Behera et al., 2013). Combustion sources (vehicles, industry, biomass burning) should contribute only a fraction of NH_3 seeing that NH_3 is not related to NOx or CO in our study. Moreover, the release of both HONO and NH_3 depend on the strength of microbial activities, fertilizing amount, and soil properties (e.g., temperature, acidity and water content of soil). Although the processes of HONO and NH_3 emission from soil may not be completely synchronized, the seasonal patterns for each should be consistent.

Until now, we can separate the sources of HONO into four parts: (1) the combustion emissions from vehicles and industries ($HONO_{emi}$) with a constant emitted HONO/NOx ratio of 0.79%; (2) the conversion of NO_2 to HONO on the ground surfaces ($HONO_{grd}$) with a constant but unknown yield x_1; (3) the conversion of NO_2 to HONO on aerosol surfaces ($HONO_{aer}$) with a $PM_{2.5}$-dependent yield ($HONO_{aer}/NO_2$); and (4) emission from soil ($HONO_{soi}$), expressed by corrected NH_3 multiplied by an unknown coefficient x_2. The corrected NH_3 is obtained by subtracting combustion emission from total observed ammonia. Ammonia from combustion is found to be proportional to simultaneous CO (Meng et al., 2011;Chang et al., 2016), and a proportion of 0.3%, which is in the lower quantile of the NH_3/CO ratios in fresh air masses (for hourly data: $NO/NO_x>0.75$; UVB=0; temperature<5℃) is used from our measurements. Substituting monthly average values of measured HONO, NO_2, $PM_{2.5}$, NH_3, and CO into Eq.(11) by assuming that $HONO_{tot}$ is equal to $HONO_{obs}$, we can get an overdetermined system of equations, which have 11 equations with 2 unknowns (excluding mean values of related parameters from February), and then we derive an approximate solution (x_1=1.89%, x_2=1.62%) by the method of ordinary least squares.

Fig. 9 shows that an average of 36% of HONO is produced heterogeneously on ground surfaces without perceptible temporal variations, but the contribution of this source is overtaken by NO_2 converting to HONO on aerosols in January (approximately 40% of HONO), and was exceeded by soil emission in July and

August (approximately 40% of HONO). The seasonal variations of HONO from different pathways at night indicate that short-term observations may just capture a small part of the total picture when exploring the source mechanisms of HONO. The total HONO concentration ($HONO_{tot}$) is the sum of derived HONO from the four sources listed above. The good correlation between $HONO_{tot}$ and $HONO_{obs}$ and the low mean normalized error of $HONO_{tot}$ to $HONO_{obs}$ reveal that our assumption on nocturnal HONO sources is reasonable. It should be noted that the slope of the linearly fitted line between $HONO_{corr}/NO_2$ and $PM_{2.5}$ in spring (r=0.74, slope=0.68‰) is much higher than that in winter (r=0.60, slope=0.20‰), but we just use a mean slope of 0.26‰ to evaluate aerosol effects throughout the year, this may be why our method underestimates HONO in March and April and overestimates HONO in January, and indicating that the mass concentration of $PM_{2.5}$ is not the only factor affecting formation of HONO on aerosols. Besides, lacking considerations of the impact of RH and temperature on NO_2-to-HONO conversion and of seasonal variations in ground surface properties, uncertainties of NO_2-to-HONO conversion mechanisms and of combustion HONO emissions, and lacking direct observation for soil emitted HONO, could all result in the bias between $HONO_{tot}$ and $HONO_{obs}$, so more studies on the detailed mechanism of various HONO sources need to be performed.

$$\begin{aligned}
&\frac{[HONO_{grd}]}{[NO_2]} = x_1 \\
&\frac{[HONO_{aer}]}{[NO_2]} = 0.26‰ \times [PM_{2.5}] \\
&\frac{[HONO_{emi}]}{[NO_x]} = 0.79\% \\
&\frac{[HONO_{soi}]}{[NH_3] - 0.3\% \times [CO]} = x_2 \\
&[HONO_{tot}] = [HONO_{emi}] + [HONO_{soi}] + [HONO_{grd}] + [HONO_{aer}]
\end{aligned} \tag{11}$$

5. Conclusions

Continuous field measurement of HONO over 1 year was conducted at the SORPES

677 station in Nanjing in the western YRD of China, from December 2017 to
678 December2018. The observed seasonal average concentrations of HONO are in the
679 range of 0.45-1.04 ppb, which are comparable to those in other urban or suburban
680 regions and appears to be of vital importance to atmospheric oxidation as the OH
681 production rate of HONO is almost 3 times as that of ozone at daytime. HONO and
682 NO_x have coincident monthly variations peaking in December and decreasing to the
683 lowest value in August, and have similar diurnal pattern with the highest value in the
684 early morning and a low point in the late afternoon, both indicating that NO_x is a
685 crucial precursor of HONO.
686
687 Combustion emissions contribute an average of 23% to nocturnal HONO
688 concentrations, with an average emission ratio $\triangle HONO/\triangle NO_x$ of 0.79%. During the
689 nighttime, the dominant source of RH-dependent HONO could be the heterogeneous
690 reaction of NO_2 on wet ground or aerosol surfaces with a mean estimated conversion
691 rate of 0.0055 h^{-1}. During the daytime, a missing HONO source with an average
692 strength of 1.04 ppb/h was identified around noon, contributing about 61% of the
693 production of HONO and seeming to be photo-enhanced. HONO released from soil is
694 adopted to discuss the seasonal changes of nocturnal HONO, and can contribute 40%
695 to HONO during summer. Ground formation provides a major part of HONO at a
696 roughly constant proportion of 36%. The uptake of NO_2 on aerosol surface could
697 generate the greatest amount of HONO during heavily polluted periods (e.g. January).
698 Our results draw a complete picture of the sources of HONO during different seasons,
699 and demonstrated the needs of long-term and comprehensive observations to improve
700 the understanding of HONO chemistry.

701 **Author contribution**

702 W.N. and A.D. designed the study; Y.L. and W.N. wrote the manuscript; Y.L., Z.X.
703 and R.X. collected the HONO data and contributed to the data analysis; T.W., Y.L.,
704 L.W. and X.C. collected other related data, e.g. NH_3, NO_x and $PM_{2.5}$.

705 **Acknowledgments**

This work was mainly funded by the National Key R&D Program of China (2016YFC0202000 and 2016YFC0200500), the National Natural Science Foundation of China (NSFC) project (D0512/41675145 and D0510/41605098), and Jiangsu Provincial Science Fund (BK20160620). Data analysis was also supported by other NSFC projects (D0512/41875175 and D0510/91644218).

References

Acker, K., Febo, A., Trick, S., Perrino, C., Bruno, P., Wiesen, P., Möller, D., Wieprecht, W., Auel, R., and Giusto, M.: Nitrous acid in the urban area of Rome, Atmos. Environ., 40, 3123-3133, 2006.

Ackermann, R.: Auswirkungen von Kraftfahrzeugemissionen in der urbanen Atmosphäre, Dissertation. de, 2000.

Alicke, B.: Impact of nitrous acid photolysis on the total hydroxyl radical budget during the Limitation of Oxidant Production/Pianura Padana Produzione di Ozono study in Milan, Journal of Geophysical Research, 107, 10.1029/2000jd000075, 2002.

Alicke, B., Platt, U., and Stutz, J.: Impact of nitrous acid photolysis on the total hydroxyl radical budget during the Limitation of Oxidant Production/Pianura Padana Produzione di Ozono study in Milan, Journal of Geophysical Research: Atmospheres, 107, LOP 9-1-LOP 9-17, 2002.

Alicke, B.: OH formation by HONO photolysis during the BERLIOZ experiment, Journal of Geophysical Research, 108, 10.1029/2001jd000579, 2003.

Ammann, M., Kalberer, M., Jost, D., Tobler, L., Rossler, E., Piguet, D., Gaggeler, H., and Baltensperger, U.: Heterogeneous production of nitrous acid on soot in polluted airmasses, NATURE, 395, 157-160, 10.1038/25965, 1998.

Ammann, M., Rossler, E., Strekowski, R., and George, C.: Nitrogen dioxide multiphase chemistry: uptake kinetics on aqueous solutions containing phenolic compounds, Phys Chem Chem Phys, 7, 2513-2518, 10.1039/b501808k, 2005.

Atkinson, R.: Atmospheric chemistry of VOCs and NOx, Atmos. Environ., 34, 2063-2101, 2000.

Atkinson, R., Baulch, D., Cox, R., Crowley, J., Hampson, R., Hynes, R., Jenkin, M., Rossi, M., and Troe, J.: Evaluated kinetic and photochemical data for atmospheric chemistry: Volume I-gas phase reactions of O x, HO x, NO x and SO x species, Atmospheric chemistry and physics, 4, 1461-1738, 2004.

Aubin, D. G., and Abbatt, J. P.: Interaction of NO2 with hydrocarbon soot: Focus on HONO yield, surface modification, and mechanism, The Journal of Physical Chemistry A, 111, 6263-6273, 2007.

Behera, S. N., Sharma, M., Aneja, V. P., and Balasubramanian, R.: Ammonia in the atmosphere: a review on emission sources, atmospheric chemistry and deposition on terrestrial bodies, Environ Sci Pollut Res Int, 20, 8092-8131, 10.1007/s11356-013-2051-9,

2013.
Bernard, F., Cazaunau, M., Grosselin, B., Zhou, B., Zheng, J., Liang, P., Zhang, Y., Ye, X., Daele, V., Mu, Y., Zhang, R., Chen, J., and Mellouki, A.: Measurements of nitrous acid (HONO) in urban area of Shanghai, China, Environ Sci Pollut Res Int, 23, 5818-5829, 10.1007/s11356-015-5797-4, 2016.
Canfield, D. E., Glazer, A. N., and Falkowski, P. G.: The Evolution and Future of Earth's Nitrogen Cycle, Science, 330, 192-196, 10.1126/science.1186120, 2010.
Chang, Y., Zou, Z., Deng, C., Huang, K., Collett, J. L., Lin, J., and Zhuang, G.: The importance of vehicle emissions as a source of atmospheric ammonia in the megacity of Shanghai, Atmospheric Chemistry and Physics, 16, 3577, 2016.
Coe, H., and Gallagher, M.: Measurements of dry deposition of NO2 to a Dutch heathland using the eddy-correlation technique, Quarterly Journal of the Royal Meteorological Society, 118, 767-786, 1992.
Cui, L., Li, R., Zhang, Y., Meng, Y., Fu, H., and Chen, J.: An observational study of nitrous acid (HONO) in Shanghai, China: The aerosol impact on HONO formation during the haze episodes, Sci Total Environ, 630, 1057-1070, 10.1016/j.scitotenv.2018.02.063, 2018.
Dillon, M. B.: Chemical evolution of the Sacramento urban plume: Transport and oxidation, 2002.
Ding, A., Nie, W., Huang, X., Chi, X., Sun, J., Kerminen, V.-M., Xu, Z., Guo, W., Petäjä, T., Yang, X., Kulmala, M., and Fu, C.: Long-term observation of air pollution-weather/climate interactions at the SORPES station: a review and outlook, Frontiers of Environmental Science & Engineering, 10, 10.1007/s11783-016-0877-3, 2016.
Ding, A. J., Fu, C. B., Yang, X. Q., Sun, J. N., Zheng, L. F., Xie, Y. N., Herrmann, E., Nie, W., Petäjä, T., Kerminen, V. M., and Kulmala, M.: Ozone and fine particle in the western Yangtze River Delta: an overview of 1 yr data at the SORPES station, Atmospheric Chemistry and Physics, 13, 5813-5830, 10.5194/acp-13-5813-2013, 2013.
Dusanter, S., Vimal, D., Stevens, P., Volkamer, R., and Molina, L.: Measurements of OH and HO2 concentrations during the MCMA-2006 field campaign–Part 1: Deployment of the Indiana University laser-induced fluorescence instrument, Atmospheric Chemistry and Physics, 9, 1665-1685, 2009.
Elshorbany, Y. F., Kurtenbach, R., Wiesen, P., Lissi, E., Rubio, M., Villena, G., Gramsch, E., Rickard, A., Pilling, M., and Kleffmann, J.: Oxidation capacity of the city air of Santiago, Chile, Atmospheric Chemistry and Physics, 9, 2257-2273, 2009.
Finlayson-Pitts, B. J., and Pitts, J. N.: CHAPTER 6 - Rates and Mechanisms of Gas-Phase Reactions in Irradiated Organic – NOx – Air Mixtures, in: Chemistry of the Upper and Lower Atmosphere, edited by: Finlayson-Pitts, B. J., and Pitts, J. N., Academic Press, San Diego, 179-263, 2000.
Finlayson-Pitts, B. J., Wingen, L. M., Sumner, A. L., Syomin, D., and Ramazan, K. A.: The heterogeneous hydrolysis of NO2 in laboratory systems and in outdoor and indoor atmospheres: An integrated mechanism, Physical Chemistry Chemical Physics, 5, 223-242, 10.1039/b208564j, 2003.
Fountoukis, C., and Nenes, A.: ISORROPIA II: a computationally efficient thermodynamic equilibrium model for K+-Ca2+-Mg2+-Nh(4)(+)-Na+-SO42--NO3--Cl--H2O aerosols, Atmospheric Chemistry and Physics, 7, 4639-4659, 10.5194/acp-7-4639-2007, 2007.

George, C., Strekowski, R. S., Kleffmann, J., Stemmler, K., and Ammann, M.: Photoenhanced uptake of gaseous NO2 on solid organic compounds: a photochemical source of HONO?, Faraday Discussions, 130, 195, 10.1039/b417888m, 2005.
Grassian, V.: Chemical reactions of nitrogen oxides on the surface of oxide, carbonate, soot, and mineral dust particles: Implications for the chemical balance of the troposphere, The Journal of Physical Chemistry A, 106, 860-877, 2002.
Han, C., Liu, Y., and He, H.: Heterogeneous reaction of NO2 with soot at different relative humidity, Environmental Science and Pollution Research, 24, 21248-21255, 10.1007/s11356-017-9766-y, 2017.
Hao, N., Zhou, B., Chen, D., and Chen, L.-m.: Observations of nitrous acid and its relative humidity dependence in Shanghai, Journal of Environmental Sciences, 18, 910-915, 10.1016/s1001-0742(06)60013-2, 2006.
Harrison, R. M., Peak, J. D., and Collins, G. M.: Tropospheric cycle of nitrous acid, Journal of Geophysical Research: Atmospheres, 101, 14429-14439, 1996.
Heland, J., ., Kleefmann, J., ., Kurtenbach, R., ., and Wiesen, P., . A new instrument to measure gaseous nitrous acid (HONO) in the atmosphere, Environmental Science & Technology, 35, 3207-3212, 2001.
Hendrick, F., Müller, J. F., Clémer, K., Wang, P., De Mazière, M., Fayt, C., Gielen, C., Hermans, C., Ma, J. Z., Pinardi, G., Stavrakou, T., Vlemmix, T., and Van Roozendael, M.: Four years of ground-based MAX-DOAS observations of HONO and NO₂ in the Beijing area, Atmospheric Chemistry and Physics, 14, 765-781, 10.5194/acp-14-765-2014, 2014.
Herrmann, H., Schaefer, T., Tilgner, A., Styler, S. A., Weller, C., Teich, M., and Otto, T.: Tropospheric aqueous-phase chemistry: kinetics, mechanisms, and its coupling to a changing gas phase, Chem Rev, 115, 4259-4334, 10.1021/cr500447k, 2015.
Hou, S., Tong, S., Ge, M., and An, J.: Comparison of atmospheric nitrous acid during severe haze and clean periods in Beijing, China, Atmos. Environ., 124, 199-206, 10.1016/j.atmosenv.2015.06.023, 2016.
Huang, R. J., Yang, L., Cao, J., Wang, Q., Tie, X., Ho, K. F., Shen, Z., Zhang, R., Li, G., Zhu, C., Zhang, N., Dai, W., Zhou, J., Liu, S., Chen, Y., Chen, J., and O'Dowd, C. D.: Concentration and sources of atmospheric nitrous acid (HONO) at an urban site in Western China, Sci Total Environ, 593-594, 165-172, 10.1016/j.scitotenv.2017.02.166, 2017.
Huang, X., Song, Y., Li, M., Li, J., Huo, Q., Cai, X., Zhu, T., Hu, M., and Zhang, H.: A high-resolution ammonia emission inventory in China, Global Biogeochemical Cycles, 26, n/a-n/a, 10.1029/2011gb004161, 2012.
Jarvis, D. L., Leaderer, B. P., Chinn, S., and Burney, P. G.: Indoor nitrous acid and respiratory symptoms and lung function in adults, Thorax, 60, 474-479, 10.1136/thx.2004.032177, 2005.
Jenkin, M. E., Cox, R. A., and Williams, D. J.: Laboratory studies of the kinetics of formation of nitrous acid from the thermal reaction of nitrogen dioxide and water vapour, Atmos. Environ., 22, 487-498, 1988.
Kalberer, M., Ammann, M., Arens, F., Gäggeler, H. W., and Baltensperger, U.: Heterogeneous formation of nitrous acid (HONO) on soot aerosol particles, Journal of Geophysical Research: Atmospheres, 104, 13825-13832, 10.1029/1999jd900141, 1999.

Kanaya, Y., Cao, R., Akimoto, H., Fukuda, M., Komazaki, Y., Yokouchi, Y., Koike, M., Tanimoto, H., Takegawa, N., and Kondo, Y.: Urban photochemistry in central Tokyo: 1. Observed and modeled OH and HO2radical concentrations during the winter and summer of 2004, Journal of Geophysical Research, 112, 10.1029/2007jd008670, 2007.

Khalizov, A. F., Cruz-Quinones, M., and Zhang, R.: Heterogeneous reaction of NO2 on fresh and coated soot surfaces, The Journal of Physical Chemistry A, 114, 7516-7524, 2010.

Kirchner, U., Scheer, V., and Vogt, R.: FTIR spectroscopic investigation of the mechanism and kinetics of the heterogeneous reactions of NO2 and HNO3 with soot, The Journal of Physical Chemistry A, 104, 8908-8915, 2000.

Kirchstetter, T., Harley, R., and Littlejohn, D.: Measurement of Nitrous Acid in Motor Vehicle Exhaust, Environmental Science & Technology Letters, 30, 2843-2849, 10.1021/es960135y, 1996.

Kleffmann, J., Becker, K., and Wiesen, P.: Heterogeneous NO2 conversion processes on acid surfaces: Possible atmospheric implications, Atmos. Environ., 32, 2721-2729, 10.1016/S1352-2310(98)00065-X, 1998.

Kleffmann, J., Becker, K. H., Lackhoff, M., and Wiesen, P.: Heterogeneous conversion of NO2 on carbonaceous surfaces, Physical Chemistry Chemical Physics, 1, 5443-5450, 1999.

Kleffmann, J.: Daytime formation of nitrous acid: A major source of OH radicals in a forest, Geophysical Research Letters, 32, 10.1029/2005gl022524, 2005.

Kleffmann, J., Lörzer, J. C., Wiesen, P., Kern, C., Trick, S., Volkamer, R., Rodenas, M., and Wirtz, K.: Intercomparison of the DOAS and LOPAP techniques for the detection of nitrous acid (HONO), Atmos. Environ., 40, 3640-3652, 10.1016/j.atmosenv.2006.03.027, 2006.

Kurtenbach, R., Becker, K., Gomes, J., Kleffmann, J., Lorzer, J., Spittler, M., Wiesen, P., Ackermann, R., Geyer, A., and Platt, U.: Investigations of emissions and heterogeneous formation of HONO in a road traffic tunnel, Atmos. Environ., 35, 3385-3394, 10.1016/S1352-2310(01)00138-8, 2001.

Lammel, G., and Cape, J. N.: Nitrous Acid and Nitrite in the Atmosphere, CHEMICAL SOCIETY REVIEWS, 25, 361-369, 10.1039/cs9962500361, 1996.

Lammel, G.: Formation of nitrous acid: parameterisation and comparison with observations, Max-Planck-Institut für Meteorologie, 1999.

Lee, J. D., Whalley, L. K., Heard, D. E., Stone, D., Dunmore, R. E., Hamilton, J. F., Young, D. E., Allan, J. D., Laufs, S., and Kleffmann, J.: Detailed budget analysis of HONO in central London reveals a missing daytime source, Atmospheric Chemistry and Physics, 16, 2747-2764, 10.5194/acp-16-2747-2016, 2016.

Li, D., Xue, L., Wen, L., Wang, X., Chen, T., Mellouki, A., Chen, J., and Wang, W.: Characteristics and sources of nitrous acid in an urban atmosphere of northern China: Results from 1-yr continuous observations, Atmos. Environ., 182, 296-306, 10.1016/j.atmosenv.2018.03.033, 2018.

Li, X., Brauers, T., Häseler, R., Bohn, B., Fuchs, H., Hofzumahaus, A., Holland, F., Lou, S., Lu, K. D., Rohrer, F., Hu, M., Zeng, L. M., Zhang, Y. H., Garland, R. M., Su, H., Nowak, A., Wiedensohler, A., Takegawa, N., Shao, M., and Wahner, A.: Exploring the atmospheric chemistry of nitrous acid (HONO) at a rural site in Southern China, Atmospheric Chemistry and Physics, 12, 1497-1513, 10.5194/acp-12-1497-2012, 2012.

Lu, K. D., Rohrer, F., Holland, F., Fuchs, H., Bohn, B., Brauers, T., Chang, C. C., Haseler, R.,

Hu, M., Kita, K., Kondo, Y., Li, X., Lou, S. R., Nehr, S., Shao, M., Zeng, L. M., Wahner, A., Zhang, Y. H., and Hofzumahaus, A.: Observation and modelling of OH and HO2 concentrations in the Pearl River Delta 2006: a missing OH source in a VOC rich atmosphere, Atmospheric Chemistry and Physics, 12, 1541-1569, 10.5194/acp-12-1541-2012, 2012.

Lu, K. D., Hofzumahaus, A., Holland, F., Bohn, B., Brauers, T., Fuchs, H., Hu, M., Haseler, R., Kita, K., Kondo, Y., Li, X., Lou, S. R., Oebel, A., Shao, M., Zeng, L. M., Wahner, A., Zhu, T., Zhang, Y. H., and Rohrer, F.: Missing OH source in a suburban environment near Beijing: observed and modelled OH and HO2 concentrations in summer 2006, Atmospheric Chemistry and Physics, 13, 1057-1080, 10.5194/acp-13-1057-2013, 2013.

Meng, X.-L., Rosenthal, R., and Rubin, D. B.: Comparing correlated correlation coefficients, Psychological bulletin, 111, 172, 1992.

Meng, Z., Lin, W., Jiang, X., Yan, P., Wang, Y., Zhang, Y., Jia, X., and Yu, X.: Characteristics of atmospheric ammonia over Beijing, China, Atmospheric Chemistry and Physics, 11, 6139-6151, 2011.

Meusel, H., Kuhn, U., Reiffs, A., Mallik, C., Harder, H., Martinez, M., Schuladen, J., Bohn, B., Parchatka, U., Crowley, J. N., Fischer, H., Tomsche, L., Novelli, A., Hoffmann, T., Janssen, R. H. H., Hartogensis, O., Pikridas, M., Vrekoussis, M., Bourtsoukidis, E., Weber, B., Lelieveld, J., Williams, J., Pöschl, U., Cheng, Y., and Su, H.: Daytime formation of nitrous acid at a coastal remote site in Cyprus indicating a common ground source of atmospheric HONO and NO, Atmospheric Chemistry and Physics, 16, 14475-14493, 10.5194/acp-16-14475-2016, 2016.

Michoud, V., Colomb, A., Borbon, A., Miet, K., Beekmann, M., Camredon, M., Aumont, B., Perrier, S., Zapf, P., Siour, G., Ait-Helal, W., Afif, C., Kukui, A., Furger, M., Dupont, J. C., Haeffelin, M., and Doussin, J. F.: Study of the unknown HONO daytime source at a European suburban site during the MEGAPOLI summer and winter field campaigns, Atmospheric Chemistry and Physics, 14, 2805-2822, 10.5194/acp-14-2805-2014, 2014.

Nie, W., Ding, A. J., Xie, Y. N., Xu, Z., Mao, H., Kerminen, V. M., Zheng, L. F., Qi, X. M., Huang, X., Yang, X. Q., Sun, J. N., Herrmann, E., Petäjä, T., Kulmala, M., and Fu, C. B.: Influence of biomass burning plumes on HONO chemistry in eastern China, Atmospheric Chemistry and Physics, 15, 1147-1159, 10.5194/acp-15-1147-2015, 2015.

Oswald, R., Behrendt, T., Ermel, M., Wu, D., Su, H., Cheng, Y., Breuninger, C., Moravek, A., Mougin, E., and Delon, C.: HONO emissions from soil bacteria as a major source of atmospheric reactive nitrogen, Science, 341, 1233-1235, 2013.

Pagsberg, P., Bjergbakke, E., Ratajczak, E., and Sillesen, A.: Kinetics of the gas phase reaction OH+ NO (+ M)→ HONO (+ M) and the determination of the UV absorption cross sections of HONO, Chemical physics letters, 272, 383-390, 1997.

Perner, D., and Platt, U.: Detection of nitrous acid in the atmosphere by differential optical absorption, Geophysical Research Letters, 6, 917-920, doi:10.1029/GL006i012p00917, 1979.

Platt, U., Perner, D., Harris, G. W., Winer, A. M., and Pitts, J. N.: Observations of nitrous acid in an urban atmosphere by differential optical absorption, Nature, 285, 312-314, 10.1038/285312a0, 1980.

Qi, X. M., Ding, A. J., Nie, W., Petäjä, T., Kerminen, V. M., Herrmann, E., Xie, Y. N., Zheng, L. F., Manninen, H., Aalto, P., Sun, J. N., Xu, Z. N., Chi, X. G., Huang, X., Boy, M., Virkkula, A., Yang, X. Q., Fu, C. B., and Kulmala, M.: Aerosol size distribution and new

particle formation in the western Yangtze River Delta of China: 2 years of measurements at the SORPES station, Atmospheric Chemistry and Physics, 15, 12445-12464, 10.5194/acp-15-12445-2015, 2015.
Rappenglück, B., Lubertino, G., Alvarez, S., Golovko, J., Czader, B., and Ackermann, L.: Radical precursors and related species from traffic as observed and modeled at an urban highway junction, Journal of the Air & Waste Management Association, 63, 1270-1286, 10.1080/10962247.2013.822438, 2013.
Reisinger, A. R.: Observations of HNO2 in the polluted winter atmosphere: possible heterogeneous production on aerosols, Atmos. Environ., 34, 3865-3874, 2000.
Richter, A., Burrows, J. P., Nuss, H., Granier, C., and Niemeier, U.: Increase in tropospheric nitrogen dioxide over China observed from space, Nature, 437, 129-132, 10.1038/nature04092, 2005.
Rohde, R. A., and Muller, R. A.: Air Pollution in China: Mapping of Concentrations and Sources, PLoS One, 10, e0135749, 10.1371/journal.pone.0135749, 2015.
Rohrer, F., and Berresheim, H.: Strong correlation between levels of tropospheric hydroxyl radicals and solar ultraviolet radiation, Nature, 442, 184-187, 10.1038/nature04924, 2006.
Rohrer, F., Lu, K., Hofzumahaus, A., Bohn, B., Brauers, T., Chang, C.-C., Fuchs, H., Häseler, R., Holland, F., Hu, M., Kita, K., Kondo, Y., Li, X., Lou, S., Oebel, A., Shao, M., Zeng, L., Zhu, T., Zhang, Y., and Wahner, A.: Maximum efficiency in the hydroxyl-radical-based self-cleansing of the troposphere, Nature Geoscience, 7, 559-563, 10.1038/ngeo2199, 2014.
Saliba, N., Yang, H., and Finlayson-Pitts, B.: Reaction of gaseous nitric oxide with nitric acid on silica surfaces in the presence of water at room temperature, The Journal of Physical Chemistry A, 105, 10339-10346, 2001.
Seinfeld, J. H., and Pandis, S. N.: Atmospheric chemistry and physics: from air pollution to climate change, John Wiley & Sons, 2016.
Shao, P., Xin, J., An, J., Kong, L., Wang, B., Wang, J., Wang, Y., and Wu, D.: The empirical relationship between PM2.5 and AOD in Nanjing of the Yangtze River Delta, Atmospheric Pollution Research, 8, 233-243, 10.1016/j.apr.2016.09.001, 2017.
Shen, Y., Virkkula, A., Ding, A., Wang, J., Chi, X., Nie, W., Qi, X., Huang, X., Liu, Q., Zheng, L., Xu, Z., Petäjä, T., Aalto, P. P., Fu, C., and Kulmala, M.: Aerosol optical properties at SORPES in Nanjing, east China, Atmospheric Chemistry and Physics, 18, 5265-5292, 10.5194/acp-18-5265-2018, 2018.
Sleiman, M., Gundel, L. A., Pankow, J. F., Jacob, P., 3rd, Singer, B. C., and Destaillats, H.: Formation of carcinogens indoors by surface-mediated reactions of nicotine with nitrous acid, leading to potential thirdhand smoke hazards, Proc Natl Acad Sci U S A, 107, 6576-6581, 10.1073/pnas.0912820107, 2010.
Sörgel, M., Regelin, E., Bozem, H., Diesch, J. M., Drewnick, F., Fischer, H., Harder, H., Held, A., Hosaynali-Beygi, Z., Martinez, M., and Zetzsch, C.: Quantification of the unknown HONO daytime source and its relation to NO2, Atmospheric Chemistry and Physics, 11, 10433-10447, 10.5194/acp-11-10433-2011, 2011.
Stemmler, K., Ammann, M., Donders, C., Kleffmann, J., and George, C.: Photosensitized reduction of nitrogen dioxide on humic acid as a source of nitrous acid, Nature, 440, 195-198, 10.1038/nature04603, 2006.
Stemmler, K., Ndour, M., Elshorbany, Y., Kleffmann, J., D'anna, B., George, C., Bohn, B.,

and Ammann, M.: Light induced conversion of nitrogen dioxide into nitrous acid on submicron humic acid aerosol, Atmospheric Chemistry and Physics, 7, 4237-4248, 2007.
Stutz, J., Kim, E. S., Platt, U., Bruno, P., Perrino, C., and Febo, A.: UV-visible absorption cross sections of nitrous acid, Journal of Geophysical Research: Atmospheres, 105, 14585-14592, 10.1029/2000jd900003, 2000.
Stutz, J., Alicke, B., and Neftel, A.: Nitrous acid formation in the urban atmosphere: Gradient measurements of NO2and HONO over grass in Milan, Italy, Journal of Geophysical Research, 107, 10.1029/2001jd000390, 2002.
Stutz, J., Alicke, B., Ackermann, R., Geyer, A., Wang, S., White, A. B., Williams, E. J., Spicer, C. W., and Fast, J. D.: Relative humidity dependence of HONO chemistry in urban areas, Journal of Geophysical Research: Atmospheres, 109, n/a-n/a, 10.1029/2003jd004135, 2004.
Su, H., Cheng, Y. F., Cheng, P., Zhang, Y. H., Dong, S., Zeng, L. M., Wang, X., Slanina, J., Shao, M., and Wiedensohler, A.: Observation of nighttime nitrous acid (HONO) formation at a non-urban site during PRIDE-PRD2004 in China, Atmos. Environ., 42, 6219-6232, 10.1016/j.atmosenv.2008.04.006, 2008a.
Su, H., Cheng, Y. F., Shao, M., Gao, D. F., Yu, Z. Y., Zeng, L. M., Slanina, J., Zhang, Y. H., and Wiedensohler, A.: Nitrous acid (HONO) and its daytime sources at a rural site during the 2004 PRIDE-PRD experiment in China, Journal of Geophysical Research, 113, 10.1029/2007jd009060, 2008b.
Su, H., Cheng, Y., Oswald, R., Behrendt, T., Trebs, I., Meixner, F. X., Andreae, M. O., Cheng, P., Zhang, Y., and Pöschl, U.: Soil nitrite as a source of atmospheric HONO and OH radicals, Science, 333, 1616-1618, 2011.
Sumner, A. L., Menke, E. J., Dubowski, Y., Newberg, J. T., Penner, R. M., Hemminger, J. C., Wingen, L. M., Brauers, T., and Finlayson-Pitts, B. J.: The nature of water on surfaces of laboratory systems and implications for heterogeneous chemistry in the troposphere, Physical Chemistry Chemical Physics, 6, 10.1039/b308125g, 2004.
Sun, P., Nie, W., Chi, X., Xie, Y., Huang, X., Xu, Z., Qi, X., Xu, Z., Wang, L., Wang, T., Zhang, Q., and Ding, A.: Two years of online measurement of fine particulate nitrate in the western Yangtze River Delta: influences of thermodynamics and N₂O₅ hydrolysis, Atmospheric Chemistry and Physics, 18, 17177-17190, 10.5194/acp-18-17177-2018, 2018.
Tan, Z., Fuchs, H., Lu, K., Hofzumahaus, A., Bohn, B., Broch, S., Dong, H., Gomm, S., Haeseler, R., He, L., Holland, F., Li, X., Liu, Y., Lu, S., Rohrer, F., Shao, M., Wang, B., Wang, M., Wu, Y., Zeng, L., Zhang, Y., Wahner, A., and Zhang, Y.: Radical chemistry at a rural site (Wangdu) in the North China Plain: observation and model calculations of OH, HO2 and RO2 radicals, Atmospheric Chemistry and Physics, 17, 663-690, 10.5194/acp-17-663-2017, 2017.
Tan, Z., Rohrer, F., Lu, K., Ma, X., Bohn, B., Broch, S., Dong, H., Fuchs, H., Gkatzelis, G. I., Hofzumahaus, A., Holland, F., Li, X., Liu, Y., Liu, Y., Novelli, A., Shao, M., Wang, H., Wu, Y., Zeng, L., Hu, M., Kiendler-Scharr, A., Wahner, A., and Zhang, Y.: Wintertime photochemistry in Beijing: observations of ROx radical concentrations in the North China Plain during the BEST-ONE campaign, Atmospheric Chemistry and Physics, 18, 12391-12411, 10.5194/acp-18-12391-2018, 2018.

1009 Tong, S., Hou, S., Zhang, Y., Chu, B., Liu, Y., He, H., Zhao, P., and Ge, M.: Comparisons of
1010 measured nitrous acid (HONO) concentrations in a pollution period at urban and suburban
1011 Beijing, in autumn of 2014, Science China Chemistry, 58, 1393-1402,
1012 10.1007/s11426-015-5454-2, 2015.
1013 Underwood, G., Song, C., Phadnis, M., Carmichael, G., and Grassian, V.: Heterogeneous
1014 reactions of NO2 and HNO3 on oxides and mineral dust: A combined laboratory and
1015 modeling study, Journal of Geophysical Research: Atmospheres, 106, 18055-18066, 2001.
1016 VandenBoer, T., Markovic, M., Sanders, J., Ren, X., Pusede, S., Browne, E., Cohen, R.,
1017 Zhang, L., Thomas, J., and Brune, W.: Evidence for a nitrous acid (HONO) reservoir at the
1018 ground surface in Bakersfield, CA, during CalNex 2010, Journal of Geophysical Research:
1019 Atmospheres, 119, 9093-9106, 2014a.
1020 VandenBoer, T. C., Young, C. J., Talukdar, R. K., Markovic, M. Z., Brown, S. S., Roberts, J.
1021 M., and Murphy, J. G.: Nocturnal loss and daytime source of nitrous acid through reactive
1022 uptake and displacement, Nature Geoscience, 8, 55-60, 10.1038/ngeo2298, 2014b.
1023 Villena, G., Kleffmann, J., Kurtenbach, R., Wiesen, P., Lissi, E., Rubio, M. A., Croxatto, G.,
1024 and Rappenglück, B.: Vertical gradients of HONO, NOx and O3 in Santiago de Chile, Atmos.
1025 Environ., 45, 3867-3873, 10.1016/j.atmosenv.2011.01.073, 2011a.
1026 Villena, G., Wiesen, P., Cantrell, C. A., Flocke, F., Fried, A., Hall, S. R., Hornbrook, R. S.,
1027 Knapp, D., Kosciuch, E., Mauldin, R. L., McGrath, J. A., Montzka, D., Richter, D., Ullmann,
1028 K., Walega, J., Weibring, P., Weinheimer, A., Staebler, R. M., Liao, J., Huey, L. G., and
1029 Kleffmann, J.: Nitrous acid (HONO) during polar spring in Barrow, Alaska: A net source of
1030 OH radicals?, Journal of Geophysical Research, 116, 10.1029/2011jd016643, 2011b.
1031 Wang, G., Zhang, R., Gomez, M. E., Yang, L., Levy Zamora, M., Hu, M., Lin, Y., Peng, J.,
1032 Guo, S., Meng, J., Li, J., Cheng, C., Hu, T., Ren, Y., Wang, Y., Gao, J., Cao, J., An, Z., Zhou,
1033 W., Li, G., Wang, J., Tian, P., Marrero-Ortiz, W., Secrest, J., Du, Z., Zheng, J., Shang, D.,
1034 Zeng, L., Shao, M., Wang, W., Huang, Y., Wang, Y., Zhu, Y., Li, Y., Hu, J., Pan, B., Cai, L.,
1035 Cheng, Y., Ji, Y., Zhang, F., Rosenfeld, D., Liss, P. S., Duce, R. A., Kolb, C. E., and Molina,
1036 M. J.: Persistent sulfate formation from London Fog to Chinese haze, Proc Natl Acad Sci U S
1037 A, 113, 13630-13635, 10.1073/pnas.1616540113, 2016.
1038 Wang, J., Zhang, X., Guo, J., Wang, Z., and Zhang, M.: Observation of nitrous acid (HONO)
1039 in Beijing, China: Seasonal variation, nocturnal formation and daytime budget, Sci Total
1040 Environ, 587-588, 350-359, 10.1016/j.scitotenv.2017.02.159, 2017.
1041 Wang, S.: Atmospheric observations of enhanced NO2-HONO conversion on mineral dust
1042 particles, Geophysical Research Letters, 30, 10.1029/2003gl017014, 2003.
1043 Wang, S., Zhou, R., Zhao, H., Wang, Z., Chen, L., and Zhou, B.: Long-term observation of
1044 atmospheric nitrous acid (HONO) and its implication to local NO2 levels in Shanghai, China,
1045 Atmos. Environ., 77, 718-724, 10.1016/j.atmosenv.2013.05.071, 2013.
1046 Wentzell, J. J. B., Schiller, C. L., and Harris, G. W.: Measurements of HONO during
1047 BAQS-Met, Atmospheric Chemistry and Physics, 10, 12285-12293,
1048 10.5194/acp-10-12285-2010, 2010.
1049 Wong, K. W., Oh, H. J., Lefer, B. L., Rappenglück, B., and Stutz, J.: Vertical profiles of
1050 nitrous acid in the nocturnal urban atmosphere of Houston, TX, Atmospheric Chemistry and
1051 Physics, 11, 3595-3609, 10.5194/acp-11-3595-2011, 2011.
1052 Xie, Y., Ding, A., Nie, W., Mao, H., Qi, X., Huang, X., Xu, Z., Kerminen, V.-M., Petäjä, T.,

Chi, X., Virkkula, A., Boy, M., Xue, L., Guo, J., Sun, J., Yang, X., Kulmala, M., and Fu, C.: Enhanced sulfate formation by nitrogen dioxide: Implications from in situ observations at the SORPES station, Journal of Geophysical Research: Atmospheres, 120, 12679-12694, 10.1002/2015jd023607, 2015.

Xu, Z., Wang, T., Xue, L. K., Louie, P. K. K., Luk, C. W. Y., Gao, J., Wang, S. L., Chai, F. H., and Wang, W. X.: Evaluating the uncertainties of thermal catalytic conversion in measuring atmospheric nitrogen dioxide at four differently polluted sites in China, Atmos. Environ., 76, 221-226, 10.1016/j.atmosenv.2012.09.043, 2013.

Xu, Z., Wang, T., Wu, J., Xue, L., Chan, J., Zha, Q., Zhou, S., Louie, P. K. K., and Luk, C. W. Y.: Nitrous acid (HONO) in a polluted subtropical atmosphere: Seasonal variability, direct vehicle emissions and heterogeneous production at ground surface, Atmos. Environ., 106, 100-109, 10.1016/j.atmosenv.2015.01.061, 2015.

Xu, Z., Huang, X., Nie, W., Chi, X., Xu, Z., Zheng, L., Sun, P., and Ding, A.: Influence of synoptic condition and holiday effects on VOCs and ozone production in the Yangtze River Delta region, China, Atmos. Environ., 168, 112-124, 10.1016/j.atmosenv.2017.08.035, 2017.

Xu, Z., Huang, X., Nie, W., Shen, Y., Zheng, L., Xie, Y., Wang, T., Ding, K., Liu, L., Zhou, D., Qi, X., and Ding, A.: Impact of Biomass Burning and Vertical Mixing of Residual-Layer Aged Plumes on Ozone in the Yangtze River Delta, China: A Tethered-Balloon Measurement and Modeling Study of a Multiday Ozone Episode, Journal of Geophysical Research: Atmospheres, 123, 11,786-711,803, 10.1029/2018jd028994, 2018.

Yabushita, A., Enami, S., Sakamoto, Y., Kawasaki, M., Hoffmann, M. R., and Colussi, A. J.: Anion-Catalyzed Dissolution of NO2 on Aqueous Microdroplets, J. Phys. Chem. A, 113, 4844-4848, 10.1021/jp900685f, 2009.

Ye, C., Zhou, X., Pu, D., Stutz, J., Festa, J., Spolaor, M., Tsai, C., Cantrell, C., Mauldin, R. L., 3rd, Campos, T., Weinheimer, A., Hornbrook, R. S., Apel, E. C., Guenther, A., Kaser, L., Yuan, B., Karl, T., Haggerty, J., Hall, S., Ullmann, K., Smith, J. N., Ortega, J., and Knote, C.: Rapid cycling of reactive nitrogen in the marine boundary layer, Nature, 532, 489-491, 10.1038/nature17195, 2016.

Ye, C., Zhang, N., Gao, H., and Zhou, X.: Photolysis of Particulate Nitrate as a Source of HONO and NOx, Environ Sci Technol, 51, 6849-6856, 10.1021/acs.est.7b00387, 2017.

Yu, Y., Galle, B., Panday, A., Hodson, E., Prinn, R., and Wang, S.: Observations of high rates of NO2-HONO conversion in the nocturnal atmospheric boundary layer in Kathmandu, Nepal, ATMOSPHERIC CHEMISTRY AND PHYSICS, 9, 6401-6415, 10.5194/acp-9-6401-2009, 2009.

Zhou, L., Wang, W., Hou, S., Tong, S., and Ge, M.: Heterogeneous uptake of nitrogen dioxide on Chinese mineral dust, J Environ Sci (China), 38, 110-118, 10.1016/j.jes.2015.05.017, 2015.

Zhou, X., Civerolo, K., Dai, H., Huang, G., Schwab, J., and Demerjian, K.: Summertime nitrous acid chemistry in the atmospheric boundary layer at a rural site in New York State, Journal of Geophysical Research: Atmospheres, 107, ACH 13-11-ACH 13-11, 10.1029/2001jd001539, 2002.

Zhou, X., Gao, H., He, Y., Huang, G., Bertman, S. B., Civerolo, K., and Schwab, J.: Nitric acid photolysis on surfaces in low-NOxenvironments: Significant atmospheric implications, Geophysical Research Letters, 30, n/a-n/a, 10.1029/2003gl018620, 2003.

Zhou, X., Zhang, N., TerAvest, M., Tang, D., Hou, J., Bertman, S., Alaghmand, M., Shepson, P. B., Carroll, M. A., Griffith, S., Dusanter, S., and Stevens, P. S.: Nitric acid photolysis on forest canopy surface as a source for tropospheric nitrous acid, Nature Geoscience, 4, 440-443, 10.1038/ngeo1164, 2011.

1141

Tables

Table 1. Sources and sinks for nitrous acid (HONO) in the troposphere.

Budget	Occurrence	Pathways	Abbr.
Sinks	Only daytime	$HONO + h\upsilon \xrightarrow{320-400nm} OH + NO$	R1
	Mainly daytime	$HONO + OH \rightarrow NO_2 + H_2O$	R2
	All day	Deposition/heterogeneous loss on aerosol	/
Sources	Mainly daytime	$NO + OH \xrightarrow{M} HONO$	R3
	Mainly nighttime	$2NO_{2(g)} + H_2O_{(ads)} \xrightarrow{surf} HONO_{(g)} + HNO_{3(ads)}$	R4
	Mainly daytime	$NO_{2(g)} + HC_{red} \xrightarrow{surf} HONO_{(g)} + HC_{ox}$	R5
	Only daytime	$HNO_3 / NO_3^- + h\upsilon \xrightarrow{surf} HONO / NO_2^- + O$	R6
	All day	Release of soil nitrite	/
	All day	Combustion emission(fossil and biomass)	/

Table 2. Overview of the measured HONO and NOx levels in Nanjing and comparison with other urban or suburban sites.

Location	Date	HONO(ppb)		NO_2(ppb)		NOx(ppb)		HONO/NO2		HONO/NOx		Ref
		Night	Day	Night	Day	Night	Day	Night	Day	Night	Day	
Rome(Italy)	May-Jun 2001	1.00	0.15	27.2	4.0	51.2	4.2	0.037	0.038	0.020	0.036	1
Kathmandu(Nepal)	Jan-Feb 2003	1.74	0.35	17.9	8.6	20.1	13.0	0.097	0.041	0.087	0.027	2
Tokto(Japan)	Jan-Feb 2004	0.80	0.05	31.8	18.2	37.4	26.3	0.025	0.003	0.021	0.002	3
Santiago(Chile)	Mar 2005	3.00	1.50	30.0	20.0	200.0	40.0	0.100	0.075	0.015	0.038	4
Mexico City(Mexico)	Mar 2006	/	0.43	/	28.4	/	44.8	/	0.015	/.	0.010	5
Houston(USA)	Sep 2006	0.50	0.10	20.0	10.0	/	/	0.025	0.010	/	/	6
Shanghai(China)	Oct 2009	1.50	1.00	41.9	30.0	/	/	0.038	0.032	/	/	7
Hongkong(China)	Aug 2011	0.66	0.70	21.8	18.1	29.3	29.3	0.031	0.042	0.025	0.028	8
	Nov 2011	0.95	0.89	27.2	29.0	37.2	40.6	0.034	0.030	0.028	0.021	
	Feb 2012	0.88	0.92	22.2	25.8	37.8	48.3	0.036	0.035	0.025	0.020	
	May 2012	0.33	0.40	14.7	15.0	19.1	21.1	0.022	0.030	0.019	0.022	
Beijing(China)	Oct–Nov 2014	1.75	0.93	37.6	35.3	94.5	53.4	0.047	0.026	0.019	0.017	9
Xi'an(China)	Jul–Aug 2015	0.51	1.57	15.4	24.7	/	/	0.033	0.062	/	/	10
Jinan(China)	Sep–Nov 2015	0.87	0.66	25.4	23.2	38.0	37.5	0.049	0.034	0.034	0.022	11
	Dec 2015-Feb 2016	2.15	1.35	41.1	34.6	78.5	64.8	0.056	0.047	0.034	0.031	
	Mar–May 2016	1.24	1.04	35.8	25.8	47.3	36.0	0.046	0.052	0.035	0.041	
	Jun–Aug 2016	1.20	1.01	22.5	19.0	29.1	25.8	0.106	0.079	0.060	0.049	
Nanjing(China)	Nov 2017-Nov 2018	0.80	0.57	18.9	13.9	24.9	19.3	0.045	0.044	0.041	0.036	this
	Dec-Feb(winter)	1.15	0.92	28.4	23.1	45.5	37.7	0.040	0.038	0.029	0.025	study
	Mar–May(spring)	0.76	0.59	17.4	12.9	19.1	15.9	0.048	0.049	0.046	0.042	
	Jun–Aug(summer)	0.56	0.34	12.5	7.7	13.5	9.1	0.048	0.051	0.046	0.045	
	Sep–Nov(autumn)	0.81	0.51	18.9	13.4	25.1	17.7	0.044	0.035	0.039	0.029	

1: Acker et al. (2006); 2: Yu et al. (2009); 3: Kanaya et al. (2007); 4: Elshorbany et al. (2009); 5: Dusanter et al. (2009); 6: Wong et al. (2011); 7: Bernard et al. (2016); 8: Xu et al. (2015); 9: Tong et al. (2015); 10: Huang et al. (2017); 11: Li et al. (2018)

Table 3. Correlations of $P_{unknown}$ against various parameters.

Parameters	Winter		Spring		Summer		Autumn	
	r	N	r	N	r	N	r	N
NO_2	0.46	220	0.33	280	0.07	366	0.15	348
$PM_{2.5}$	0.41	220	0.43	280	0.22	366	0.26	348
NO_3^-	0.39	211	0.41	270	-0.01	353	0.19	344
SO_4^{2-}	0.34	204	0.26	270	0.15	357	0.23	337
NH_4^+	0.38	211	0.36	273	0.09	360	0.22	332
RH	0.00	220	-0.33	280	-0.37	366	-0.19	348
UVB	0.22	220	0.44	280	0.43	366	0.45	348
NO_2*$PM_{2.5}$	0.42	220	0.43	280	0.10	366	0.23	348
NO_2*NO_3^-	0.40	211	0.43	270	-0.04	353	0.20	344
NO_2*SO_4^{2-}	0.41	204	0.35	270	0.08	357	0.22	337
NO_2*NH_4^+	0.41	211	0.41	273	0.05	360	0.21	332
UVB*NO_2	0.59	220	0.68	280	0.49	366	0.65	348
UVB*$PM_{2.5}$	0.53	220	0.64	280	0.51	366	0.65	348
UVB*NO_3^-	0.50	211	0.56	270	0.25	353	0.46	344
UVB*SO_4^{2-}	0.42	204	0.49	270	0.42	357	0.55	337
UVB*NH_4^+	0.47	211	0.53	273	0.35	360	0.52	332
NO_2*UVB*$PM_{2.5}$	0.53	220	0.64	280	0.39	366	0.55	348

Figures

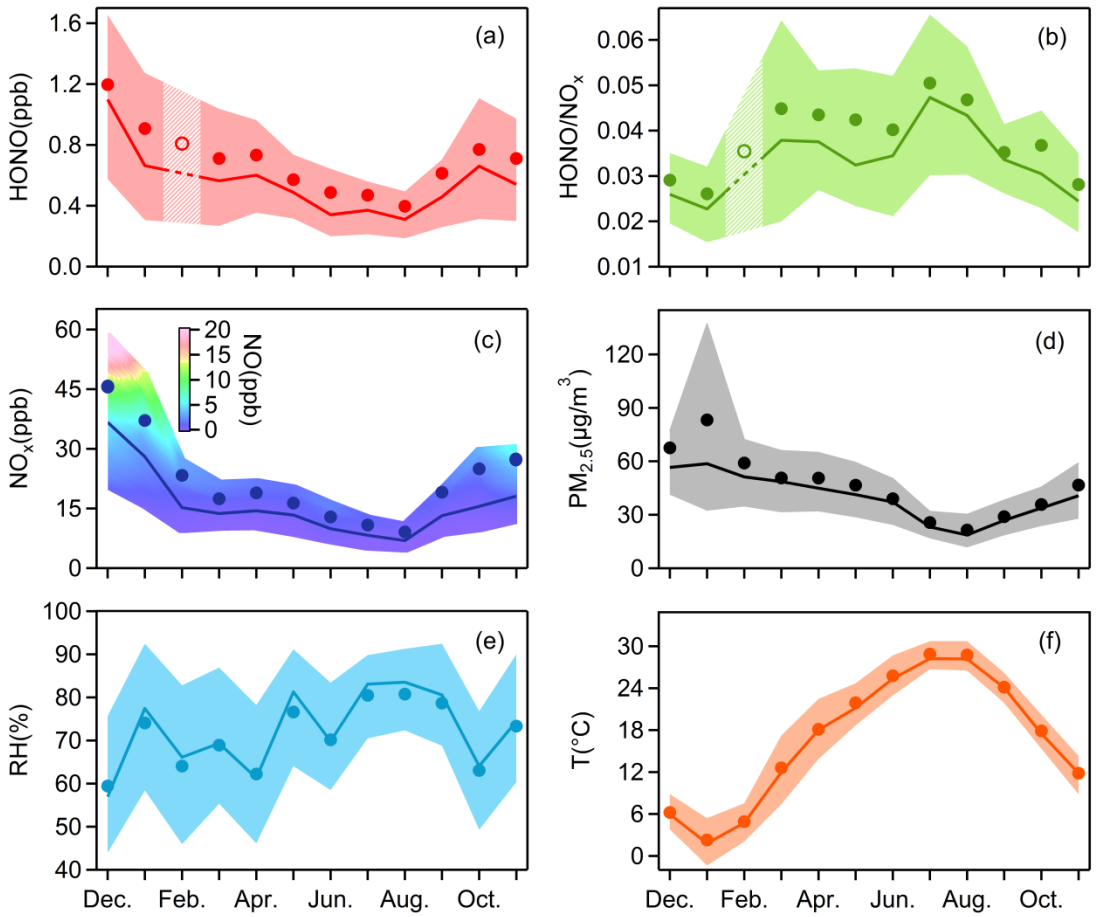

Fig. 1. Monthly variations of (a) HONO, (b) HONO/NO_x, (c) NO_x, (d) $PM_{2.5}$, (e) RH and (f) T. The solid bold lines are median values, the markers indicate mean values, and the shaded areas represent percentiles of 75% and 25%. In (a) and (b), values in February are linearly interpolated based on the data from the months before and after, since there were only few days when HONO was observed in February. In (c), the shaded area is colored by the 25_{th} to the 75_{th} percentiles of NO.

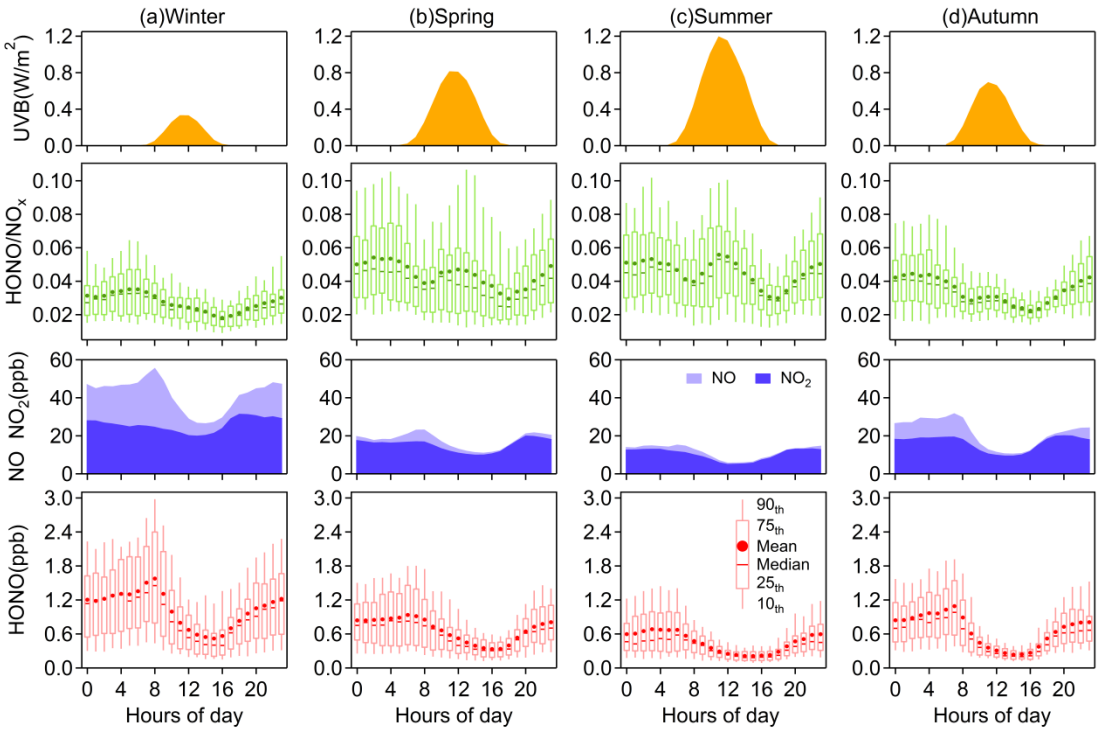

Fig. 2. Diurnal variations of HONO, NO, NO_2, HONO/NO_x, UVB in (a) winter, (b) spring, (c) summer, (d) autumn. The levels of NO, NO_2 and UVB are displayed as their mean concentrations.

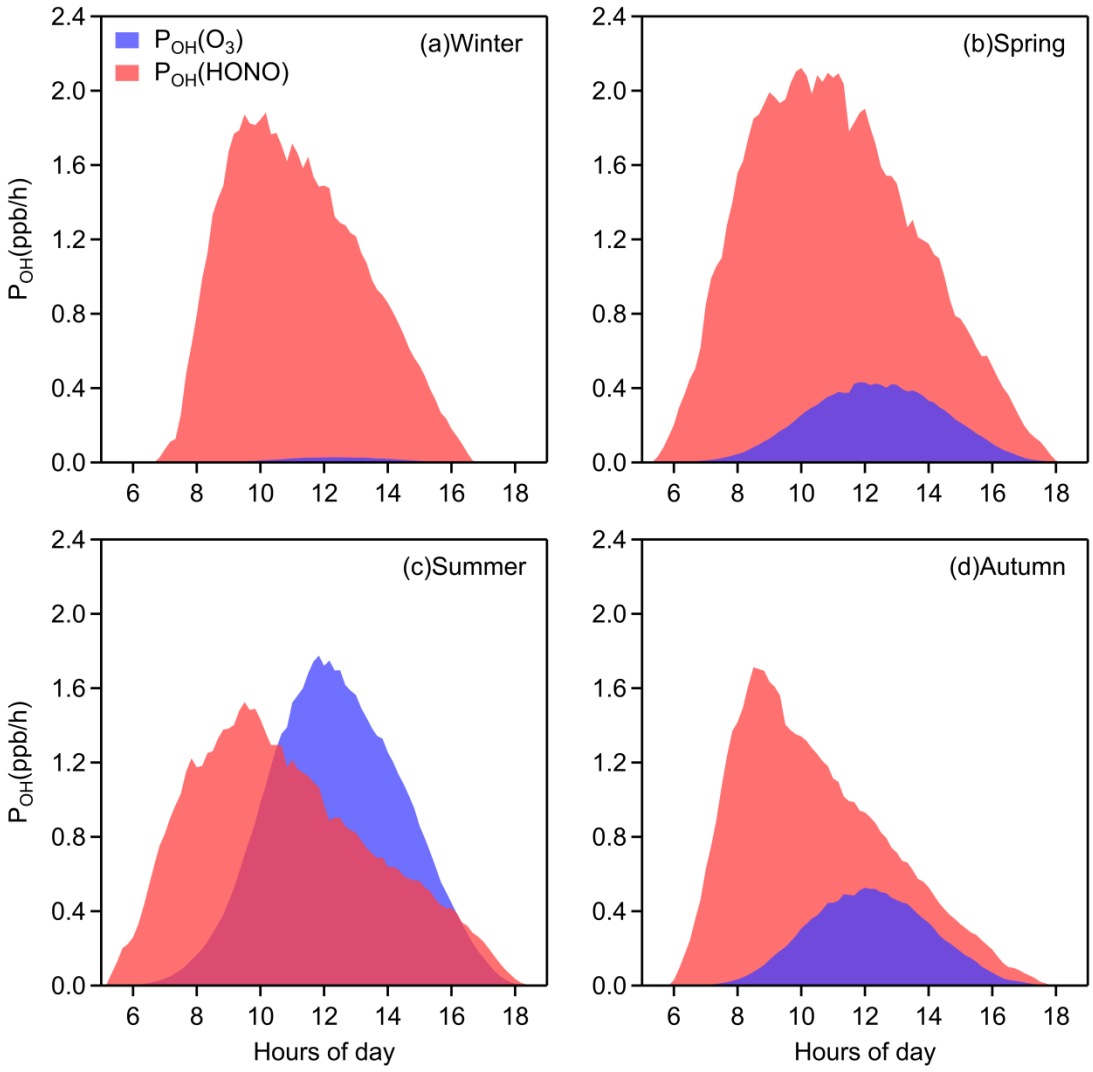

Fig. 3. Averaged OH production rates from photolysis of HONO and ozone in (a) winter, (b) spring, (c) summer, and (d) autumn.

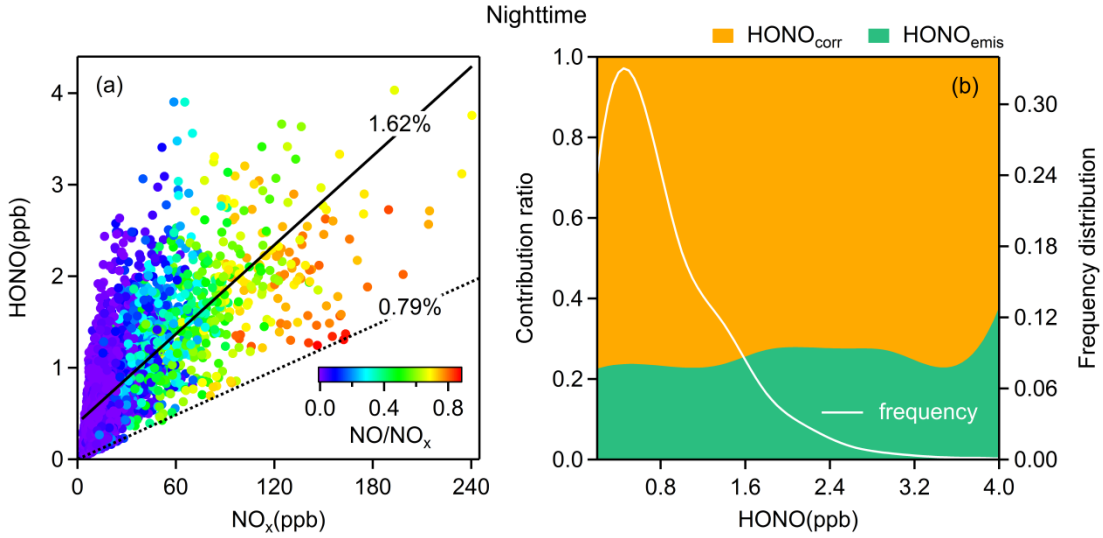

Fig. 4. (a) The relationship between HONO and NO_x colored by the NO/NO_x ratio. The dotted line is the emission ratio derived in this study and the solid line is obtained from simple linear fitting; (b) average emission contribution ratios for different concentrations of HONO and the frequency distribution of HONO concentrations. Both (a) and (b) are nighttime values.

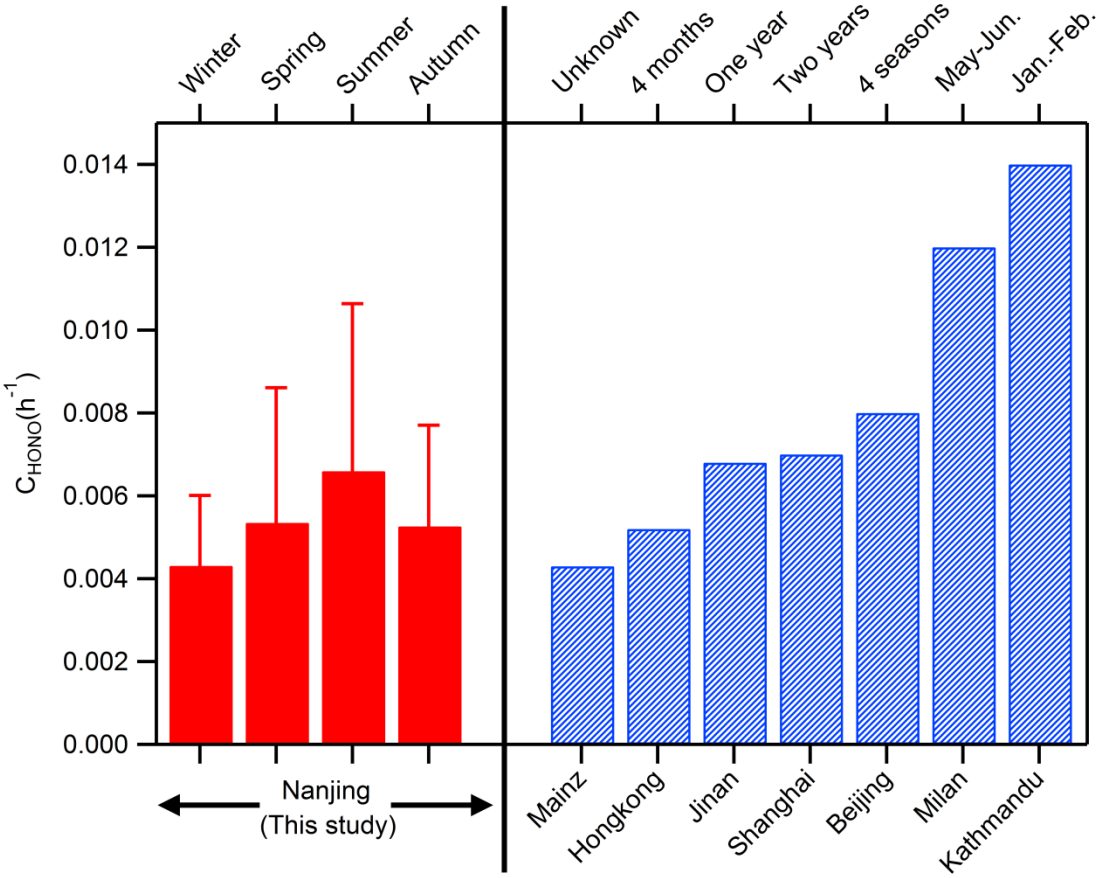

1176

Fig. 5. Comparison of observed NO_2 to HONO conversion rates in cities: Nanjing (this study); Mainz (Lammel, 1999); Hongkong (Xu et al., 2015); Jinan (Li et al., 2018); Shanghai (Wang et al., 2013); Beijing (Wang et al., 2017); Milan (Alicke et al., 2002); and Kathmandu (Yu et al., 2009).

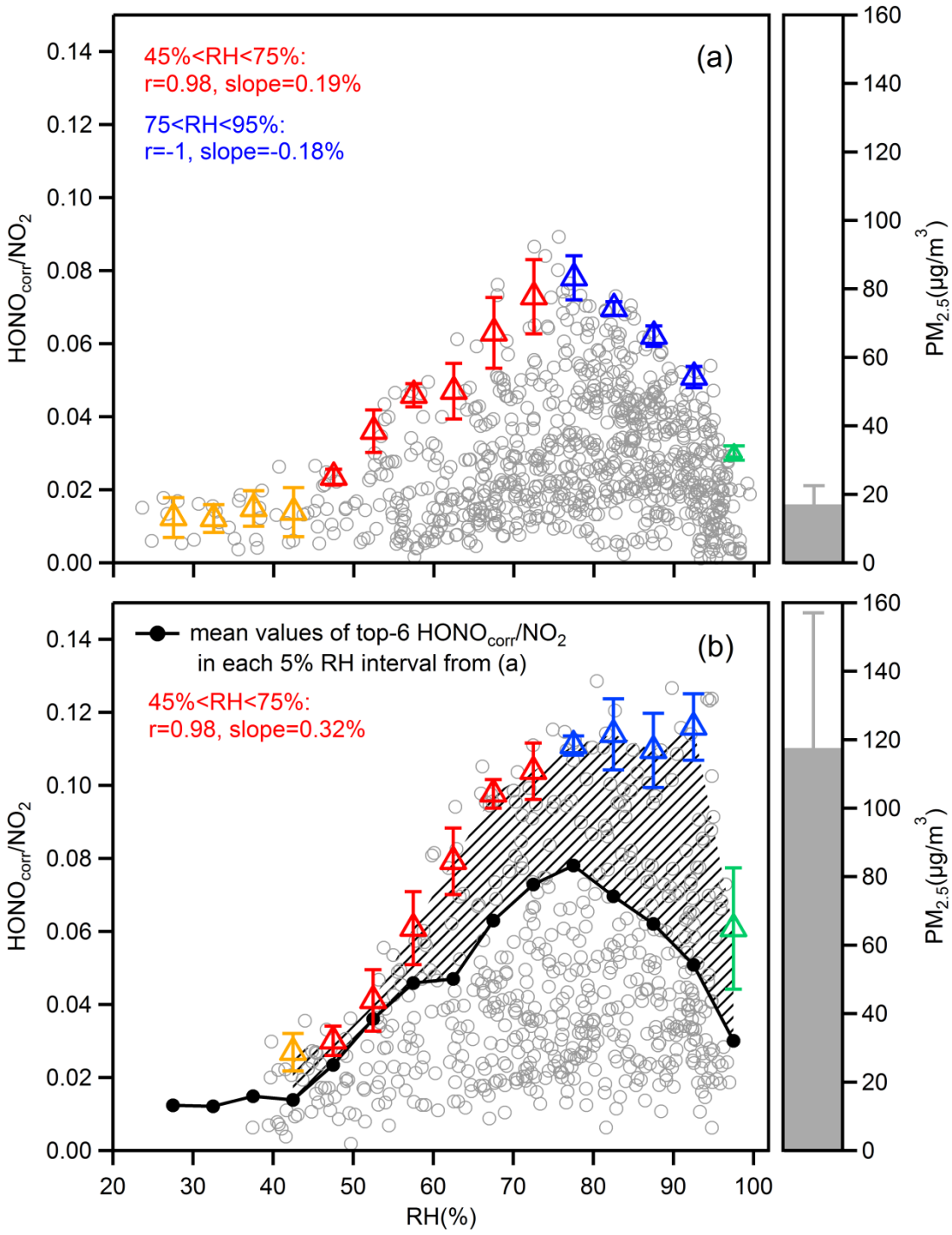

Fig. 6. Scatter plot of the $HONO_{corr}/NO_2$ ratio and RH during nighttime, separating the data into (a) clean hours (hourly mean $PM_{2.5}$<25μg/m^3) and (b) polluted hours (hourly mean $PM_{2.5}$>75μg/m^3). Triangles are the averaged top-6 $HONO_{corr}$/NO2 in each 5% RH interval, and the error bars are the standard deviations. The overall average concentrations of $PM_{2.5}$ in (a) and (b) are shown to the right of the figures.

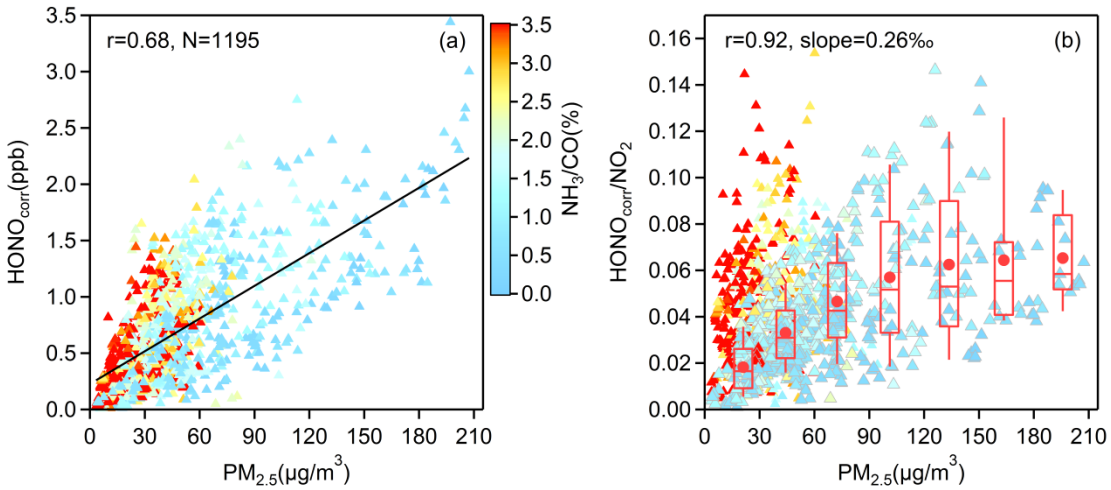

Fig. 7. (a) The correlation between $HONO_{corr}$ and $PM_{2.5}$, and (b) the correlation between $HONO_{corr}/NO_2$ and $PM_{2.5}$, all scatters come from the time (3:00-6:00 LT) when the $HONO_{corr}/NO_2$ ratio reaches the pseudo steady state at each night and are colored by NH_3/CO. In (b), the larger triangles with gray borders, depict the measured data from November to May, and the boxplot in each 30 μg/m^3 interval of $PM_{2.5}$ is illustrated according to the same data, the red box boundaries represent interquartile range, the whiskers represent the 10%–90% percentile range, the horizontal red lines represent median values and the red markers represent mean values. The correlation coefficient and the slope of the linearly fitted line in (b) are derived from the averaged $HONO_{corr}/NO_2$ and averaged $PM_{2.5}$ in each box.

1177

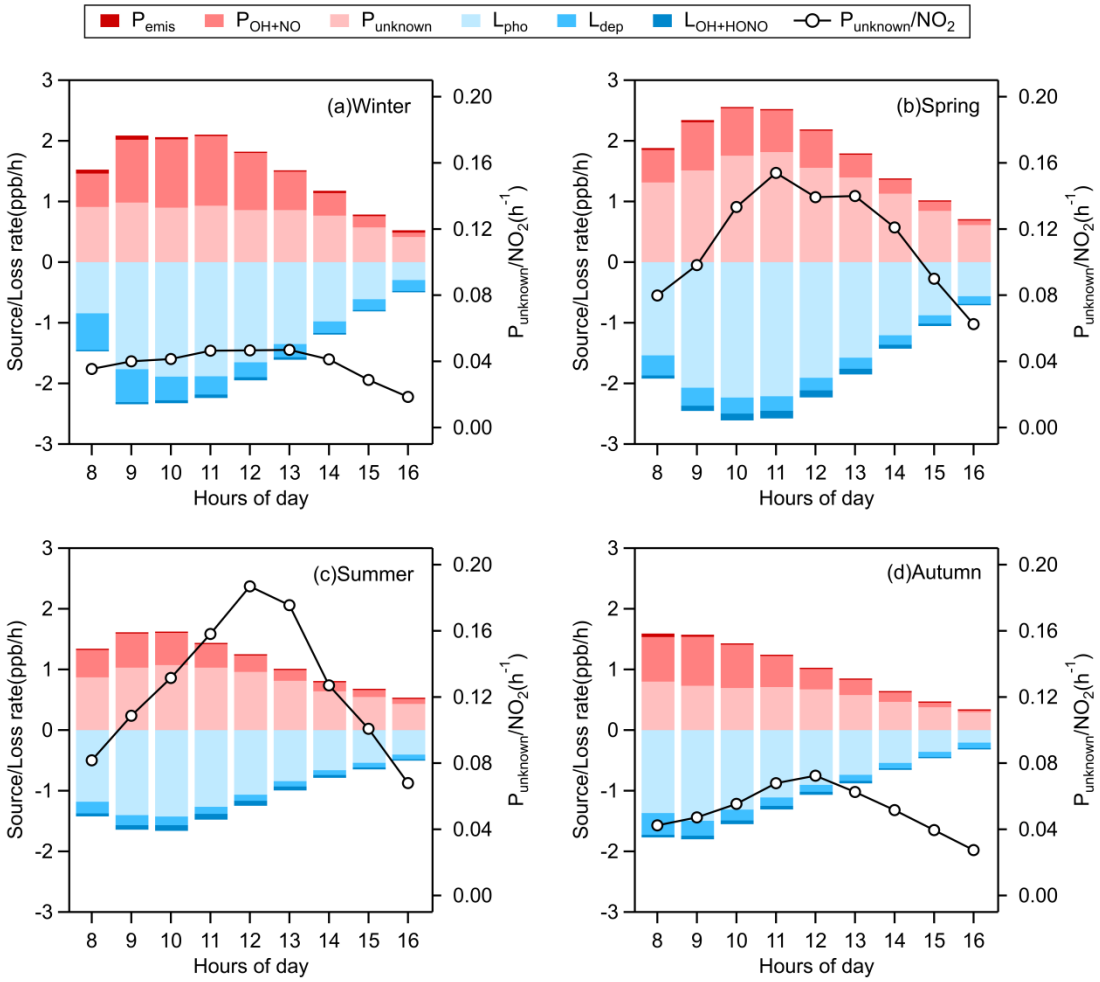

Fig. 8. Averaged daytime HONO budget and the missing source strength ($P_{unknown}$) normalized by NO_2 in (a) winter, (b) spring, (c) summer, and (d) autumn. The mean values of $P_{unknown}$ around noontime (10:00-14:00 LT) are: 0.91 ppb/h in winter, 1.61 ppb/h in Spring, 0.98 ppb/h in summer, 0.68 ppb/h in autumn.

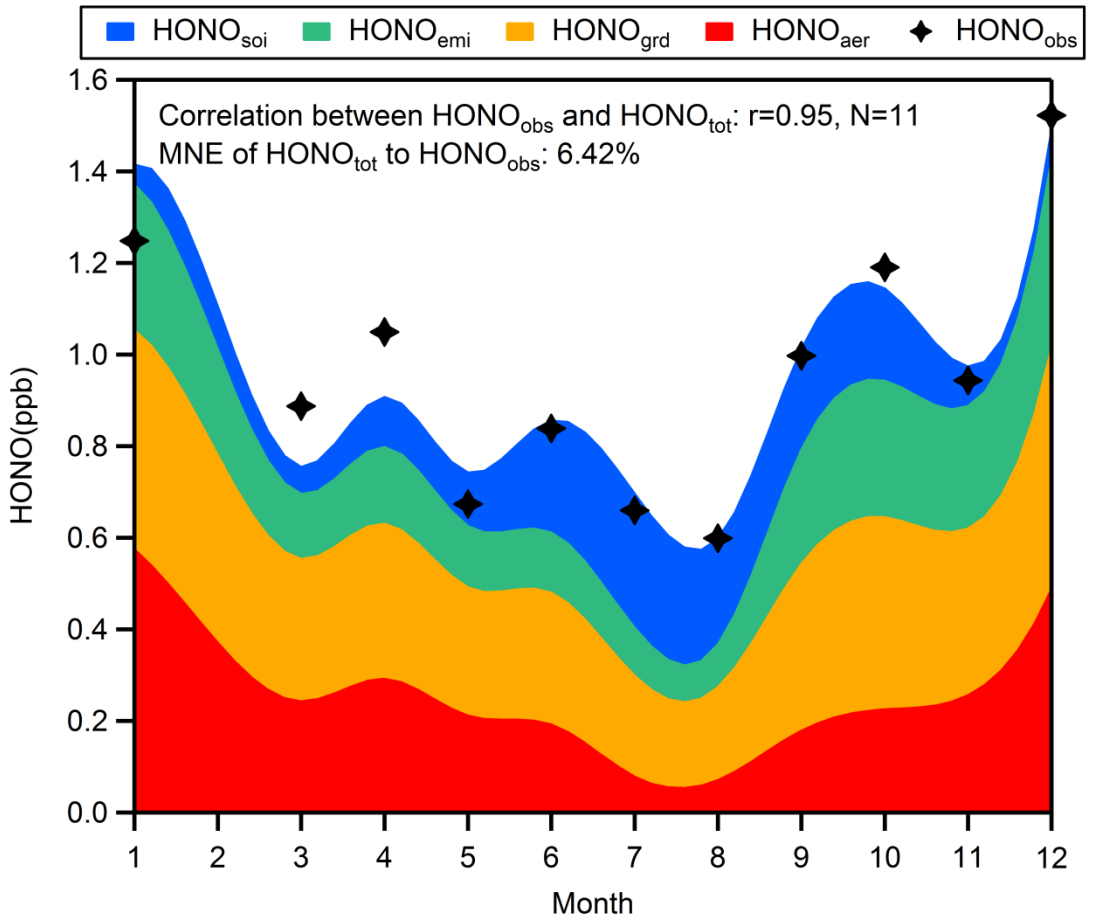

Fig. 9. Seasonal variations of 4 sources of HONO at night (3:00-6:00 LT).The mean normalized error (MNE) of $HONO_{tot}$ to $HONO_{obs}$ is 6.42%.